THESIS

TEMPORAL CHANGES IN THE CYTOSOLIC PROTOEME OF THE PROXIMAL CONVOLUTED TUBULE DURING THE ONSET OF METABOLIC ACIDOSIS

Submitted by

Kevin Lee Schauer

Department of Biochemistry and Molecular Biology

In partial fulfillment of the requirements

For the Degree of Master of Science

Colorado State University

Fort Collins, Colorado

Spring 2013

Master's Committee:

Advisor: Norman P. Curthoys

Jessica E. Prenni
Gregory L. Florant

ABSTRACT

TEMPORAL CHANGES IN THE CYTOSOLIC PROTOEME OF THE PROXIMAL CONVOLUTED TUBULE DURING THE ONSET OF METABOLIC ACIDOSIS

A decrease in blood pH coupled with a decrease in blood bicarbonate concentration is a relatively common pathological condition that is referred to as metabolic acidosis. The proximal convoluted tubule cells in the kidney respond to this condition by increasing the extraction of plasma glutamine, and up-regulating ammoniagenesis and gluconeogenesis. These processes produce bicarbonate ions that are transported to the blood to help restore acid-base homeostasis. A few cytosolic proteins such as phosphoenolpyruvate carboxykinase have previously been identified to play a role in the renal response to metabolic acidosis, but further analysis is needed to better characterize the response of the entire proteome. Therefore, proximal convoluted tubule cells were isolated from rat kidney cortex tissue at various times after onset of acidosis and fractionated to separate the soluble cytosolic proteins from the remainder of the cellular components. The cytosolic proteins were analyzed using two-dimensional liquid chromatography tandem mass spectrometry to identify the constituent proteins. Spectral counting along with average MS/MS total ion current was used to quantify temporal changes in relative protein abundance. In all, 461 proteins were confidently identified in the samples, of which 24 exhibited statistically significant changes in abundance. To validate the technique, several of the abundance changes observed by spectral counting were confirmed via western blotting. Data from the cytosolic fractions were then combined with previous proteomic data and bioinformatics analysis was performed to better characterize the overall changes that occur in the proximal convoluted tubule during the onset of metabolic acidosis.

ACKNOWLEDGEMENTS

I would like to start by thanking Dr. Norm Curthoys for the tremendous amount of help and support that he has provided to me over the past couple of years. I am incredibly fortunate that he was willing to allow me into his lab as a volunteer when I emailed him out of the blue one day, and then eventually take me in as a master's student. I could not have asked for a better advisor than Norm, as he was always around to give advice, but also allowed me to pursue my own interests and to conduct my research the way I chose. I would also like to thank Lynn Taylor, the lab manager and "lab mom" for the Curthoys lab for her nearly constant assistance and question answering, as well as for always making sure that the supplies I needed for my research were there when I needed them. In addition to Norm, my entire committee has been very helpful throughout the duration of the project. They have always been willing to meet with me and offer advice, and have given me a lot of helpful input throughout. Thank you Norm, Jessica and Florant!

Next, I would like to thank the entire staff of the Proteomics and Metabolomics Facility here at CSU for not only providing me with employment throughout my tenure as a master's student, but also for their constant advice and friendship. Jessica, Carolyn and Deanna have been tremendous to work for, and I can honestly say that I love my job, and there is nowhere else at CSU that I would rather work. The experience and knowledge I have gained during my time at the PMF has shaped me for the rest of my life, and I look forward to future collaborations with the facility.

I would also like to thank my family for their unwavering support. My parents have always allowed me to pursue my own path in life, and have provided me with the tools I need to succeed. I am forever thankful for their love and compassion and I will miss them tremendously

as I move on with my life and have to leave Colorado. In addition to my family, I have been fortunate enough to have a number of tremendous friends that have made my time at CSU not only educational, but also very enjoyable.

I owe more than I could ever say to my wonderful girlfriend Lily, who suggested that I get contact Norm in the first place after having him as an advisor in undergrad. Lily was always there for me whether I needed to complain, vent, or if I had a hard decision to make. I am so lucky to have someone as wonderful and loving as Lily in my life.

Last, but certainly not least, I would like to thank Dr. Dana Freund for mentoring me on my project. Dana has truly been the perfect mentor, and there is no way I could have completed the following research without her. She was always patient with my regular mistakes and willing to explain even the simplest of concepts over and over again. The majority of what I have learned in the lab is directly due to Dana's teachings, and I cannot thank her enough. I wish her the best of luck in her future research as a post doc, and I hope we can maintain our friendship well into the future.

TABLE OF CONTENTS

INTRODUCTION

Metabolic acidosis (MA) is a relatively common clinical condition that is characterized by a decrease in blood pH and bicarbonate concentration (7, 11). Numerous conditions can lead to acidosis including the excess production of ketone bodies (diabetic ketoacidosis), kidney disease, the excessive loss of bicarbonate ions that occurs with severe diarrhea, or the buildup of lactic acid (5). The kidney is a key contributor to the whole body response to regain acid-base balance. In the absence of acidosis, the kidney extracts very little of the circulating plasma glutamine (40). However, during acidosis the proximal convoluted tubule (PCT) extracts more than one-third of the plasma glutamine in a single pass through the kidneys (6, 37). This glutamine is catabolized in the PCT, forming two molecules of ammonia and two molecules of bicarbonate per glutamine (45). The resulting ammonium molecules are primarily transported across the apical membrane via the apical Na^+/H^+ exchanger type 3 (NHE-3) and are eventually excreted in the urine (6). The bicarbonate ions are returned to the blood via a basolateral Na^+-$3HCO_3^-$ cotransporter (6). The result is a net excretion of acids and an increase in blood bicarbonate, which increases the buffering capacity of the blood.

Although many of the primary responses of the PCT to MA are well characterized, much is still unknown about what other changes occur in the PCT and how such responses are regulated. In order to truly understand the whole cell response to acidosis, a global approach must be employed to simultaneously monitor the many changes that are occurring in the cell. Nowik et al. (32) used a genome wide expression profiling technique to monitor changes in the mouse renal transcriptome during the onset of acidosis. They identified nearly 13,000 transcripts in the whole kidney and found that over 4,000 mRNAs were differentially expressed during

acidosis compared to controls. However, changes in the transcriptome do not necessarily produce corresponding changes in protein expression or activity (12).

Mass spectrometry (MS) based proteomics offers the unique advantage of being able to monitor the levels of many different proteins simultaneously, which allows researchers to understand functional differences that are occurring in a system. MS-based proteomics techniques have been utilized previously in renal research (21, 23). Much of the earlier proteomics work utilized gel-based techniques such as two-dimensional gel electrophoresis (7, 23), but recently, the use of liquid chromatography tandem mass spectrometry (LC-MS/MS) has proven to be a valuable tool (11, 43, 44). This method allows for a more comprehensive view of the whole proteome, and also overcomes many of the problems associated with gel-based techniques such as the need for long periods of optimization, bias towards hydrophilic proteins, and lack of reproducibility (13, 21).

Previous work has used proteomics techniques to characterize the proteome of the rat PCT, as well as its response to MA (7, 11, 43, 44). However, the complexity of the PCT proteome made it difficult to analyze the response of the entire cell simultaneously. Thus, previous studies used cellular fractionation to simplify the samples prior to MS analysis (11, 43, 44). This approach allowed for more in-depth analysis of the proteome, but left several fractions unanalyzed. To date, the apical membrane (43, 44) and mitochondrial (11) proteomes have been analyzed, but no work has focused on the cytosolic proteins. Yet, it is well established that much of the response of the PCT to MA involves processes that occur primarily in the cytosol such as gluconeogenesis and mRNA stabilization (6). To address this knowledge gap, the study presented here is focused on proteome characterization of cytosolic fractions from PCT cells isolated from both acidotic and control rats.

MATERIALS AND METHODS

Animals

All samples were collected from male Sprague-Dawley rats between 6 and 12 weeks of age that were purchased from Charles River Laboratories (Kingston, NY). Rats were provided with free access to rodent chow (Harlan-Tekland, Madison, WI) throughout the duration of the study. Control rats were provided with normal tap water, where experimental rats were made acidotic by providing 0.28 M NH_4Cl as their sole source of drinking water for a period of 1, 3 or 7 days (hereafter referred to as acutely acidotic, acidotic, or chronically acidotic, respectively). Fluid consumption was checked daily to ensure that all of the acidotic rats consumed a volume of NH_4Cl at least as great as the water consumed by the control rats. In addition, acutely acidotic rats were stomach loaded with 20 mmol/kg of body weight of NH_4Cl at the start of treatment. Previous work has established that this protocol produced a pronounced metabolic acidosis in the acutely acidotic and acidotic animals that is partially compensated in the chronically acidotic rats (44). Three control (non-acidotic) rats, as well as three biological replicates per acidotic time point were used, for a total of 12 animals. All animals were randomly assigned to their respective treatment groups. All procedures were approved by the Institutional Animal Care and Use Committee at Colorado State University.

Isolation of Proximal Convoluted Tubules and Soluble Cytosolic Fractions

The procedure for the isolation of rat renal proximal convoluted tubules (PCT) has been described previously (11, 43). In brief, the renal cortex was dissected from freshly sacrificed animals and submitted to collagenase digestion in a buffer containing 1 mM phenylmethanesulfonylfluoride (PMSF) to inhibit protease activity. PCT were then separated by Percoll density gradient centrifugation. Isolated PCT were pelleted via a 10 minute, 1000xg spin

at 4°C and resuspended in 0.3 M sucrose with 1 mM PMSF, 12 mM HEPES, and 1 mM EDTA. Resuspended PCT were homogenized using a 5 ml Teflon homogenizer. The resulting homogenate was centrifuged twice at 700xg for 10 minutes to remove nuclei and cell debris, and then again for 10 minutes at 7,000xg to pellet a crude mitochondrial fraction. Finally, the samples were centrifuged at 100,000xg for 20 minutes at 4ºC to pellet the remaining organelles. The supernatants from this spin contained the soluble cytosolic fractions that were used for further analyses. All samples were stored at -80ºC in 1 mM PMSF and freeze-thaw cycles were avoided to limit protein degradation.

Western Blotting Analyses

A total of 8 μg of protein (unless otherwise noted) was separated by 10% or 15% SDS-PAGE depending on if the target protein was larger or smaller than 40 kDa, respectively. Separated proteins were then transferred to a polyvinylidene fluoride (PVDF) membrane and incubated for a minimum of two hours in Pierce Protein-Free (TBS) Blocking Buffer (Thermo Scientific, Rockford, IL). Blocking buffer was removed and membranes were incubated overnight in a dilute solution of primary antibody in blocking buffer. Depending on the host species of the primary antibody, either 680 Dylight-conjugated goat anti-rabbit or 800 Dylight-conjugated goat anti-mouse was used as a secondary antibody. Membranes were imaged using an Odyssey Infrared Imager (LI-COR Biosciences, Lincoln, NE) and bands were quantified using the accompanying Image Studio software.

Determination of Cytosolic Sample Purity

In order to determine the purity of the cytosolic fractions, western blotting was used to quantify the depletion of soluble, organelle-specific proteins between the PCT lysates and the cytosolic fractions. Depletion of these organelle-specific proteins was interpreted as a measure of

purity for the cytosolic fractions. Three crude homogenates taken from isolated rat renal proximal convoluted tubules and three cytosolic samples obtained from control animals (non-acidotic) were subjected to western blotting. Antibodies specific to cathepsin B (EMD Millipore, Billerica, MA), aconitase 2 (Aviva Systems Biology, San Diego, CA), binding immunoglobulin protein (BiP) (Cell Signaling Technology, Danvers, MA), and cAMP response element-binding protein 1 (CREB-1) (Santa Cruz Biotechnolgy, Santa Cruz, CA) were used for the analysis. The antibodies react with soluble proteins that are localized specifically to lysosomes, mitochondria, endoplasmic reticula, and nuclei, respectively.

Sample Preparation for Mass Spectrometry Analysis

Cytosolic fractions were dialyzed into 50 mM NH_4HCO_3 and their concentrations determined by bicinchoninic acid (BCA) assay (38). Aliquots containing 50 μg of each of the control, 1-day acutely acidotic, and 7-day chronically acidotic samples were subjected to tryptic digestion to prepare for analysis by mass spectrometry (MS). Briefly, proteins were precipitated by acetone precipitation and then resolubilized in 8 M urea by bath sonication for 5 minutes. ProteaseMAX surfactant trypsin enhancer (Promega, Madison, WI) was added to a final concentration of 0.2%. Disulfide bonds were then reduced with dithiothrietol, and alkalyated with iodoacetamide. Proteins were digested for 3 h at 37°C using Trypsin Gold mass-spectrometry grade protease (Promega, Madison, WI). The digestion was halted by the addition of trifluoroacetic acid to a final concentration of 0.5% and samples were dried in a vacuum evaporator. The resulting peptides were purified using a C18 TopTip (Glygen, Columbia, MD) and dried again using a vacuum evaporator. Dried peptides were resuspended in 3% acetonitrile/0.1% formic acid immediately prior to MS analysis.

Mass Spectrometry Analysis

Sample fractionation was performed using an online two-dimensional liquid chromatography (2D-LC) system. A 10-µg aliquot of digested peptides was injected directly onto a strong-cation exchange (SCX) column (ZORBAX BioSCX Series II, 800 µm x 50 mm, 3.5 µm column, Agilent Technologies, Santa Clara, CA). Elution from the SCX column was performed by the injection of 20 µl salt bumps of 30, 40, 50, 60, 90, and 500 mM NaCl. Peptides eluted from the SCX column were temporally separated on a subsequent reverse phase, C18 column (1200 nanoHPLC, Zorbax C18, 5 µm, 75 µm ID x 150 mm column, Agilent Technologies, Santa Clara, CA) using a 90-minute linear gradient from 25% to 55% of 90% acetonitrile/0.1% formic acid solution. Flow rates were maintained at 300 nl/min throughout the gradient.

Peptides eluted from the reverse phase column traveled directly into the linear ion trap mass spectrometer (LTQ, Thermo Scientific, Rockford, IL). Spectra were collected using a mass window of 200-2000 m/z. A dynamic exclusion limit was used that allowed for a maximum of 2 MS/MS spectra for a given peptide in 30 seconds, followed by a 90 second exclusion of that peptide. Compound lists of the resulting spectra were compiled using Xcaliber 2.2 software (Thermo Scientific, Rockford, IL) with an intensity threshold of 5,000 and 1 scan per group. Ion chromatograms were monitored throughout data collection to ensure instrument functionality and consistency. In addition, tryptic digests of bovine serum albumin were injected between each sample as a quality control.

Bioinformatics

Tandem mass spectra (MS/MS) were searched against a Uniprot-KB *Rattus norvegicus* reverse-concatenated database (downloaded December, 21 2011) using both Mascot (version

2.3.02, Matrix Science) and SEQUEST (version v.27, rev. 11, Sorcerer, Sage-N Research) search algorithms. The reverse database was searched in order to calculate false discovery rates (FDR) as described previously (8). Search parameters were as follows: average mass, 2.5 Da peptide mass tolerance, 1.0 Da fragment ion mass tolerance, complete tryptic digestion with a maximum of two missed cleavages per peptide, a static modification of cysteine carbamidomethylation, and variable modifications of methionine oxidation and lysine acetylation. Search results were loaded into Scaffold 3 software (Version 3.6.0, Proteome Software, Portland, OR) for analysis.

Filters were applied such that only proteins with 99% minimum protein probability, 95% minimum peptide probability, and at least two unique peptides were included in the dataset. Protein and peptide probabilities were calculated using the Peptide and Protein Prophet algorithms included in the Scaffold 3 software (22, 30). Scaffold 3 software was also used to assign peptides shared between proteins to satisfy the laws of parsimony. Spectra from proteins identified by only two assigned unique peptides were manually validated using the following criteria: presence of at least 3 sequential y and b ions in the same spectrum, or at least 5 consecutive ions (either y or b) with at least 5% relative intensity, as well as a lack of prominent unassigned peaks.

Relative Protein Abundance Determination

Both spectral counting (SpC) and average total ion current of the MS/MS (MS^2 TIC) were used as measures of relative abundance. The two methods were previously shown to be complimentary (10). Spectral counting uses the sum of MS/MS spectra assigned to each protein as a measure of abundance, where average MS^2 TIC uses the average ion intensity across all peptides for a particular protein to estimate abundance. These values were used to calculate fold changes, and were subjected to statistical tests to determine which of the observed changes were

significant. The data were first normalized using the method embedded in the Scaffold software that has been described previously (1). In brief, a scaling factor was created by dividing the total number of spectra identified in a sample by the mean of spectra identified across all samples in the analysis. The SpC values for each of the proteins in the sample were then divided by this scaling factor. MS^2 TIC values were normalized in the same way, but SpC values were replaced with MS/MS total ion current.

Statistical Analysis

One-way ANOVA was performed on the normalized values using DanteR (41), an R-based proteomics software, to determine which proteins showed significant abundance changes in samples from acidotic rats compared to those from controls. The ANOVA model used by DanteR was developed specifically for proteomics studies, and has been shown to accurately detect changes in such datasets (33). Fold changes for the SpC data were calculated by first adding a pseudo count of one to all the quantitative values (in order to remove zeros) and then the mean value for each treatment was divided by the mean control value. MS^2 TIC fold changes were calculated in the same manner, with the exception that a pseudo count value of 506 (the lowest detected MS^2 TIC value in the dataset) was used instead of one. Proteins were considered to be differentially expressed in a treatment if they had a significant p-value ($p < 0.05$) and showed at least a 1.5 fold change as compared to controls.

Validation of Proteomics Data

A subset of the proteins found to be differentially expressed in the mass spectrometry analysis were validated via western blotting. All western blotting procedures were completed as explained above. The following proteins were validated by western blotting: cytosolic phosphoenolpyruvate carboxykinase (PEPCK), glutathione S-transferase P1 (GSTP1), aconitase

1 (ACO1), phenylalanine hydroxylase (PAH), sodium potassium ATPase alpha 1 (AT1A1), retinoid-inducible serine carboxypeptidase (RISC), glycerol kinase (GK), D-dopachrome decarboxylase (DDT), and prostaglandin E-synthase 3 (PTGES3). Antibodies specific to GSTP1, PAH and AT1A1were purchased from Novus Biologicals (Littleton, CO), while the ACO1, GK, and DDT antibodies were from Abcam (Cambridge, MA). PEPCK and RISC antibodies were produced by Abgent and Acris (San Diego, CA), respectively. Glyceraldehyde 3-phosphate dehydrogenase (GAPDH) (GeneTex, Irvine, CA) was used as a loading control for all blots. A total of 8 μg of protein was loaded for each of the control, acutely acidotic (1 day), acidotic (3 day), and chronically acidotic (7 day) biological replicates (n=3) with the exception of the AT1A1 and PAH blots where 12 μg was loaded. All blots were run in duplicate and the data was combined into one analysis.

Renal Hypertrophy

Rats obtained from Charles River Laboratories (Kingston, NY) that had either undergone a sham procedure, or a uninephrectomy (UNX) of the left kidney were used in order to determine if the observed protein abundance changes observed in the acidotic samples were due to the renal hypertrophy associated with acidosis (26) or the decrease in pH itself. The removal of one kidney was previously shown to cause a greater hypertrophy in the remaining kidney than what occurs during acidosis (36). Kidneys dissected from the uninephrectomized rats were 36% larger on average than kidneys from the sham operated animals. Rats were sacrificed 21 days post operation in order to achieve maximum renal hypertrophy, and soluble cytosolic protein samples were collected from PCT cells. Western blotting was performed as described above to determine if renal hypertrophy altered the levels of PEPCK, GSTP1, ACO1, PAH, AT1A1 or RISC levels.

Pathway Analysis

A variety of tools were used in order to group proteins that were found to be differentially regulated during acidosis into different cellular pathways and molecular functions. Gene ontology (GO) terms are a collection of descriptors that are standardized in order to allow for clear annotation of genes and proteins across all fields of research. Scaffold 3 software has built in tools that allow for easy extraction of GO annotations for proteins that are annotated in the Uniprot-KB database. This functionality was used to determine the cellular location of proteins identified in the cytosolic dataset. For some analysis, the acquired knowledge of the authors was used to group the narrowly specified GO terms into broader classifications. In addition, the Search Tool for the Retrieval of Interacting Genes/Proteins (STRING) is a freely available, web-based software that detects and maps known as well as predicted protein-protein interactions (39). STRING uses a variety of protein annotation databases including the GO database, the Kyoto Encyclopedia of Genes and Genomes (KEGG), as well as other methods to map protein interactions. This software was used to visualize protein interactions between proteins that were found to be differentially regulated during acidosis, which was useful in determining what cellular processes and pathways are affected by acidosis in the PCT. In addition, STRING allows users to download the raw annotation data that the software uses to create its maps. This output was further used to elucidate the response of PCT as a whole to acidosis.

RESULTS

Isolation of Soluble Cytosolic Proteins from Proximal Convoluted Tubules

PCT were isolated from rat renal cortex by Percoll gradient centrifugation (43). Previous work has shown that this method yields PCT that are approximately 95% pure (7, 43). Soluble cytosolic fractions were obtained by a differential centrifugation procedure that concluded with a 20 min 100,000xg spin, which should pellet the remaining organelles, leaving only the soluble cytosolic proteins. Western blot analysis was used to determine the purity of the resulting cytosolic fractions. Primary antibodies specific to cathepsin B, aconitase 2, binding immunoglobulin protein (BiP) and cAMP response element-binding protein 1 (CREB-1) were used to quantify the relative abundance of the respective proteins in the crude PCT homogenates and cytosolic fractions. These proteins were chosen because they are soluble proteins that specifically localize to lysosomes, mitochondria, the endoplasmic reticulum and nucleus, respectively, of intact cells. Thus, their depletion in the cytosolic fractions as compared to whole cell lysates is a measure of the disruption of the various organelles and the purity of the cytosolic fraction. Western blotting results found a 90% or greater depletion of these proteins in the cytosolic fractions as compared to crude PCT homogenates (Fig. 1). By contrast, greater than 95% of the initial GAPDH was recovered in the cytosolic fraction. In addition, SDS-PAGE analysis of the samples showed a multitude of proteins remaining with a wide range of molecular weights (data not shown). Taken together, these data strongly suggest that the differential centrifugation procedure successfully enriched the soluble cytosolic proteins without appreciable release of soluble proteins from various organelles. Analysis of the acidotic samples showed similar enrichment of the cytosolic fractions (data not shown).

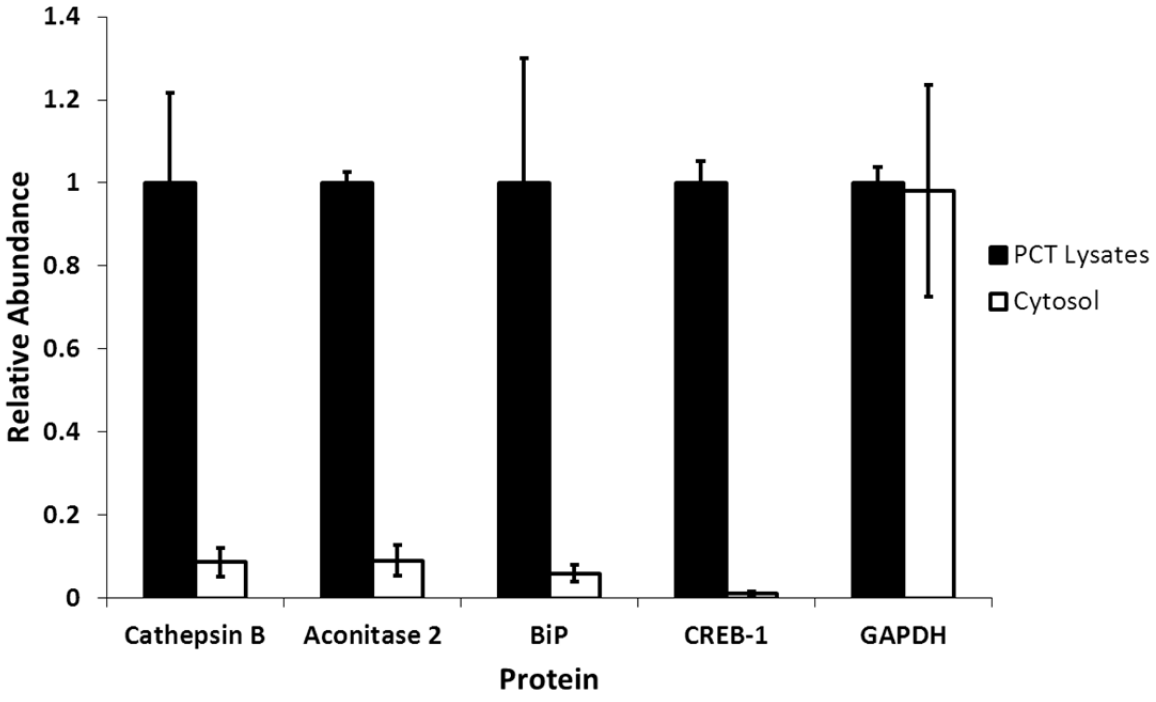

Fig. 1. Comparison of organelle specific protein levels in PCT lysates and soluble cytosolic fractions as determined by western blotting. Cathepsin B, aconitase 2, binding immunoglobulin protein (BiP) and cAMP response element binding protein 1 (CREB-1) are soluble proteins that are contained specifically in lysosomes, mitochondria, ER and nuclei, respectively. Levels of glyceraldehyde 3-phosphate dehydrogenase (GAPDH) were also quantified to illustrate the retention of a cytosolic protein in the fractions.

Mass Spectrometry Analysis of Soluble Cytosolic Fractions

Cytosolic fractions were obtained from three biological replicates of rats that were non-acidotic (control), acutely acidotic (1 day), acidotic (3 day), or chronically acidotic (7 day). Aliquots of these samples were submitted to trypsin digestion in preparation for MS analysis with the exception of the 3 d, acidotic samples. Digested peptides were then analyzed using two-dimensional liquid chromatography coupled to tandem mass spectrometry (2D-LC-MS/MS). Raw MS data were searched against a reverse concatenated *Rattus norvegicus* database using both MASCOT and SEQUEST protein search engines. In all, 91,044 identified spectra led to the identification of 461 proteins between all of the analyzed samples. The dataset had a 0.1% peptide false discovery rate (FDR) and a 2.2% protein FDR. The number of peptides and proteins identified in each sample was found to be similar across all samples (data not shown). A full list of the identified proteins is available in Table 4 of Appendix I, as well as in a searchable online format at http://helixweb.nih.gov/ESBL/Database/PCT/ (17). Scaffold 3 software was used to extract gene ontology terms for the identified proteins. Cellular location GO terms were available for 348 of the 461 proteins. Of those with annotations, 73% were cytosolic and another 8% percent were ribosomal or cytoskeletal, which would also be enriched in fractionation procedure (Fig. 2).

Relative Quantitation of Protein Abundance

A combination of spectral counting (SpC) and average MS/MS total ion current (MS^2 TIC) was used to estimate the relative abundance of proteins in the PCT following different treatments. SpC uses the number of identified MS/MS spectra assigned to a particular protein as a measure of abundance (31, 48), whereas average MS^2 TIC is based on the average ion intensity

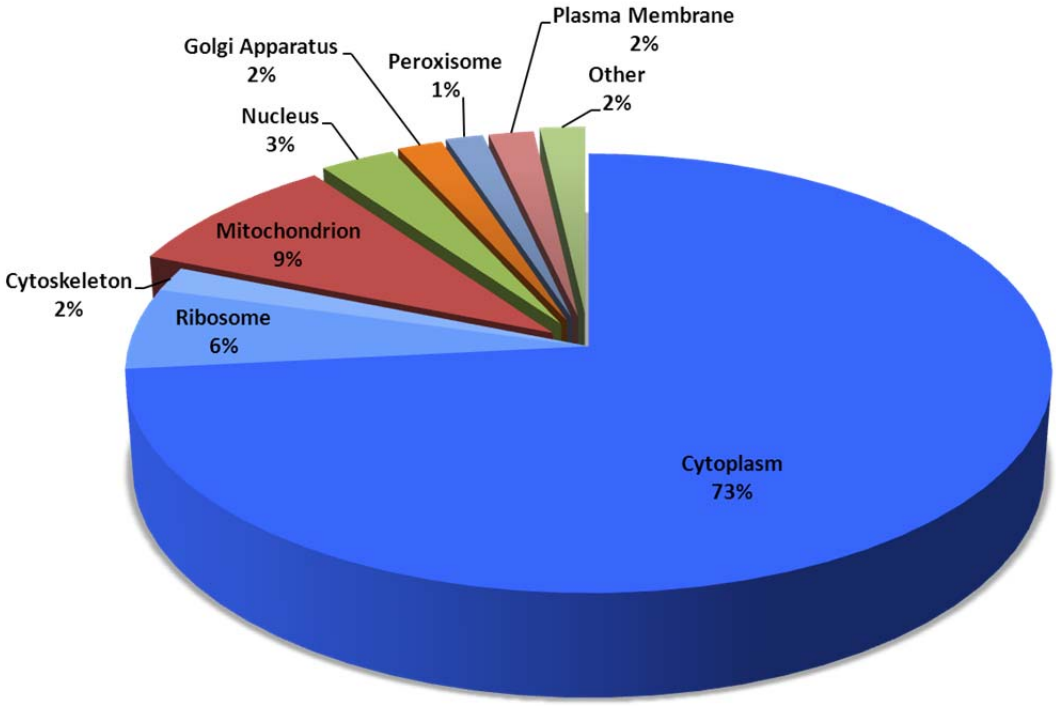

Fig. 2. Gene ontology (GO) cellular location terms for proteins identified in the cytosolic fractions derived from isolated PCT. Only proteins that were annotated with a cellular location (348 out of 471 identified) are represented here. Sections colored blue contain proteins that we would expect to be enriched in the cytosolic fractions. Proteins were grouped into the other category if there were less than 3 proteins sharing the same cellular location annotation.

of the MS/MS spectra for each peptide assigned to a given protein (3). Previous work has suggested that the two methods are complimentary, relative quantitation techniques (personal communication from D.M. Freund and J.E. Prenni). Prior to statistical analysis, the data were normalized as explained in the Materials and Methods section. In order to elucidate which proteins exhibited significant changes in abundance during acidosis, p-values were calculated by ANOVA and relative fold changes were calculated by dividing the average SpC or MS^2 TIC value for a protein in a particular treatment by the same value for the control samples. A protein was considered to be significantly altered if the comparison had both a p-value < 0.05 and a fold change of 1.5 or greater (<0.67 for decreasing proteins).

Of the 461 identified proteins, 24 were found to be differentially expressed in the cytosolic fractions in at least one time point compared to control PCT. Of those, 10 were significant only in the acutely acidotic samples (Table 1), 9 in only the chronically acidotic samples (Table 2), and 5 in both conditions. Further, SpC detected more differentially regulated proteins at both time points, with 10 proteins being identified in the acutely acidotic samples, and 9 in the chronic acidotic. Interestingly, only retinoid-inducible serine carboxypeptidase (RISC) in the acutely acidotic samples met the cut-offs for significance by both methods in the same time point. However, SpC indicated a significant increase, whereas MS^2 TIC identified a decrease.

Validation of MS Data

A subset of the proteins identified by MS as being differentially expressed during acidosis were validated by western blotting. In all, primary antibodies were obtained that were specific to: cytosolic phosphoenolpyruvate carboxykinase (PEPCK), glutathione S-transferase P (GSTP1), aconitase 1 (ACO1), phenylalanine-4-hydroxylase (PAH), sodium/potassium-transporting ATPase subunit alpha-1 (AT1A1), RISC, D-dopachrome decarboxylase (DDT) and

Table 1: Differentially regulated cytosolic proteins during acute metabolic acidosis

Protein Name	Acession Number	Entry Name	Gene Name	p-value (SpC/TIC)*	Fold Change (SpC/TIC)*	Detection Method
Phosphoenolpyruvate carboxykinase, cytosolic [GTP]	P07379	PCKGC_RAT	Pck1	0.001	4.94	SpC
Sodium/potassium-transporting ATPase subunit alpha-1	P06685	AT1A1_RAT	Atp1a1	0.003	0.10	SpC
Prostaglandin E synthase 3	P83868	TEBP_RAT	Ptges3	0.005	3.73	SpC
Low-density lipoprotein receptor-related protein 2	P98158	LRP2_RAT	Lrp2	0.008	0.33	SpC
Phenylalanine-4-hydroxylase	P04176	PH4H_RAT	Pah	0.012	0.49	SpC
Aconitase 1	D4ACL3	D4ACL3_RAT	Aco1	0.013	2.27	SpC
RCG32401, isoform CRA_a	D3ZPA9	D3ZPA9_RAT	Ctsa	0.014	4.60	SpC
WD repeat-containing protein 1	Q5RKI0	WDR1_RAT	Wdr1	0.024	3.53	SpC
6-phosphogluconolactonase	P85971	6PGL_RAT	Pgls	0.025	0.33	SpC
Ubiquitin-conjugating enzyme E2M (UBC12 homolog, yeast) (Predicted), isoform CRA_a	D3ZNQ6	D3ZNQ6_RAT	Ube2m	0.034	2.49	SpC
Retinoid-inducible serine carboxypeptidase	Q920A6	RISC_RAT	Scpep1	0.011/0.049	1.88/0.42	Both
Peroxisomal 2,4-dienoyl-CoA reductase	Q9Z2M4	DECR2_RAT	Decr2	0.009	0.17	TIC
Pyruvate carboxylase, mitochondrial	P52873	PYC_RAT	Pc	0.010	2.56	TIC
3-hydroxyisobutyrate dehydrogenase, mitochondrial	P29266	3HIDH_RAT	Hibadh	0.014	5.25	TIC
40S ribosomal protein S3	P62909	RS3_RAT	Rps3	0.027	2.35	TIC

* For proteins with significant SpC and TIC p-values, both are reported.

Proteins in bold and italics were previously identified to exhibit altered expression during acute acidosis (7, 11, 32, 44).

Table 2: Differentially regulated cytosolic proteins during chronic metabolic acidosis

Protein Name	Acession Number	Entry Name	Gene Name	p-value	Fold Change	Detection Method
Sodium/potassium-transporting ATPase subunit alpha-1	P06685	AT1A1_RAT	Atp1a1	0.003	0.14	SpC
Low-density lipoprotein receptor-related protein 2	P98158	LRP2_RAT	Lrp2	0.010	0.36	SpC
Phosphoenolpyruvate carboxykinase, cytosolic	P07379	PCKGC_RAT	Pck1	0.012	3.37	SpC
Triosephosphate isomerase	P48500	TPIS_RAT	Tpi1	0.020	0.54	SpC
Glutathione S-transferase P	P04906	GSTP1_RAT	Gstp1	0.026	3.15	SpC
Transgelin-2	Q5XFX0	TAGL2_RAT	Tagln2	0.027	0.46	SpC
Uncharacterized protein	D3ZPL5	D3ZPL5_RAT	RGD1562953	0.041	3.07	SpC
N-acylglucosamine 2-epimerase	F1LQ78	F1LQ78_RAT	Renbp	0.047	0.23	SpC
Acyl-coenzyme A thioesterase 1	O88267	ACOT1_RAT	Acot1	0.047	0.48	SpC
D-dopachrome decarboxylase	P80254	DOPD_RAT	Ddt	0.031	5.47	TIC
Aromatic-L-amino-acid decarboxylase	P14173	DDC_RAT	Ddc	0.016	0.28	TIC
Prostaglandin E synthase 3	P83868	TEBP_RAT	Ptges3	0.039	15.86	TIC
Ketohexokinase	Q02974	KHK_RAT	Khk	0.040	2.09	TIC
Pyruvate carboxylase, mitochondrial	P52873	PYC_RAT	Pc	0.045	2.05	TIC

Proteins in bold and italics were previously identified to exhibit altered expression during chronic acidosis (7, 11, 32, 44).

prostaglandin E synthase 3 (PTGES3). Triplicate biological replicates from each time point, including the acidotic (3 day) samples, were blotted together and probed with one of the antibodies described above, as well as an antibody specific for glyceraldehyde 3-phosphate dehydrogenase (GAPDH) which was used as a loading control. Blots were probed with fluorescently labeled secondary antibodies and imaged using an infrared imager. A representative blot (each blot was run in duplicate) is shown in Figure 3A. Fluorescence intensities were quantified and used as a measure of relative protein abundance. Overall, the western blot data correlated quite well with the MS data (Fig. 3B). Time courses showing the levels of each protein during the progression of acidosis are shown in Figures 3C and 3D.

Effects of Renal Hypertrophy

It is well established that metabolic acidosis causes hypertrophy of the PCT (26, 34). In order to determine if the observed changes in protein abundance during the progression of acidosis was due to renal hypertrophy or the decrease in blood pH, rats were obtained that had either undergone a sham procedure or a uninephrectomy (UNX) where the left kidney was removed (n=3 per treatment). The removal of one kidney causes a renal hypertrophy that is greater than that which occurs during acidosis (36). Twenty-one days post operation, kidneys were removed and soluble cytosolic fractions were collected using the same method as used for the acidotic animals. The samples were then analyzed in duplicate by western blotting to determine the relative levels of PEPCK, GSTP1, ACO1, PAH, AT1A1 and RISC between treatments. These proteins were chosen because both MS and western blotting showed similar changes in abundance during the development of acidosis. A representative blot from each analysis is shown in Figure 4A, along with quantification from the experiments (Fig. 4B). Overall, no difference was observed between treatments for any of the analyzed proteins, except

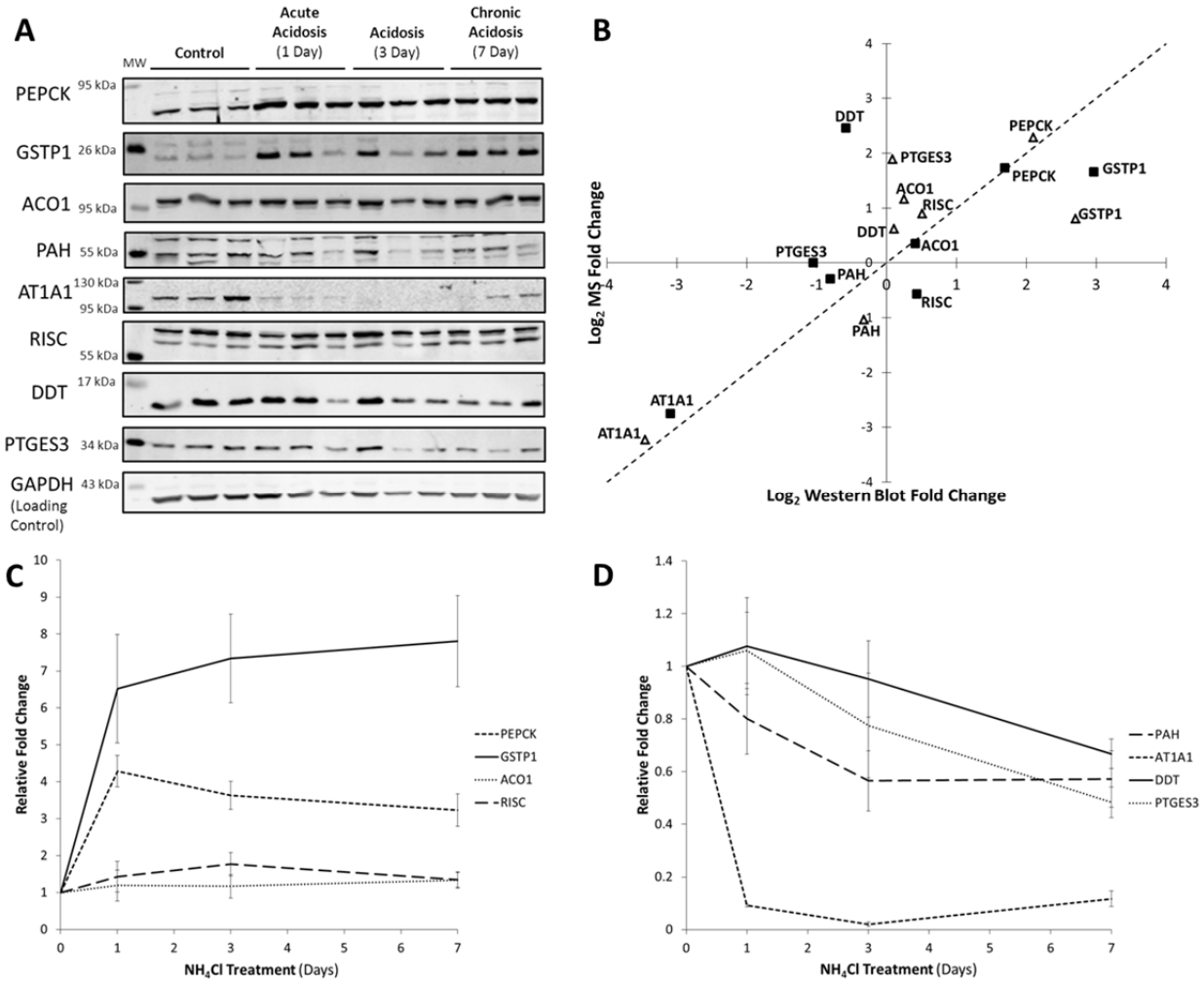

Fig. 3. Validation of MS data by western blotting. **A)** Representative blots for each of the proteins analyzed. **B)** Comparison of fold changes for acute (△) and chronic (■) acidotic samples compared to controls, as determined by MS and western blotting analysis. The MS fold changes shown are those calculated using the method (SpC/TIC) in which the protein was found to be significantly altered. In the case of RISC, the fold change calculated by SpC was used, as it had the lower p-value. **C,D)** Temporal changes in protein abundance during the progression of acidosis as determined by western blotting.

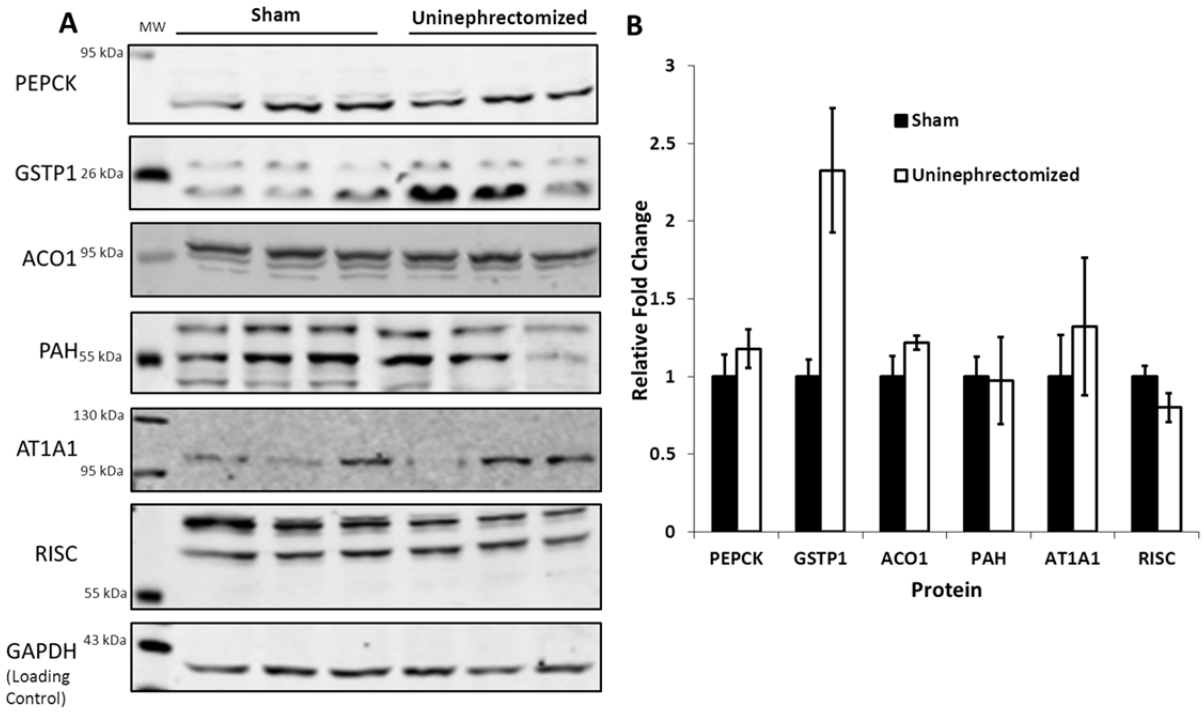

Fig. 4. The effects of renal hypertrophy on the levels of proteins that exhibit differential expression during metabolic acidosis. Cytosolic samples were prepared from rats that had undergone a sham operation or a uninephrectomy. Protein levels were measured by western blotting. **A)** Representative blots for each of the proteins analyzed. **B)** Quantification of the relative levels of each protein.

for GSTP1. Levels of GSTP1 were approximately 2-fold higher in the UNX samples as compared to controls. Although this increase is significant, it is unlikely that hypertrophy alone was responsible for the nearly 8-fold increase in GSTP1 that was observed by western blot analysis of chronically acidotic samples.

Detection of Acetylated Peptides

Previous work has suggested that variability in lysine acetylation may play a role in the response of the PCT to metabolic acidosis as well as other cellular processes (11, 47). Soluble cytosolic fractions from each treatment were blotted and probed with a primary antibody specific to acetylated lysine residues. Although a number of acetylated proteins were observed, quantification revealed no significant differences in the total number of acetylated lysines between treatments (unpublished data, D.M. Freund). Nonetheless, the MS data was searched with a variable acetyl lysine modification in order to identify sites of acetylation in cytosolic proteins in the PCT. It is important to note that due to the small mass difference between lysine acetylation and trimethylation, the ability to differentiate between the two modifications was outside the limitations of the linear ion trap mass spectrometer used in this study. Therefore, the sites identified as acetylated may actually be trimethylated. In total, 15 different acetylated/trimethylated peptides were identified across all of the analyzed samples, 9 of which have not been previously identified (Table 3). No single acetylated peptide was detected more than 5 times in any treatment.

Bioinformatic Analysis of Combined Subcellular Enrichment Data Characterizing the Response of the PCT to Acidosis

Previous studies have used MS-based proteomics to study the response of apical membrane (44) and mitochondrial (11) proteins of the PCT to acidosis. To determine how the

Table 3: Acetylated proteins detected in the cytosolic fractions

Protein Name	Accession Number	Gene Name	Number of Modified Spectra			Peptide Sequence	Modified Site*	Site Determining Ion	Novel
			Control	Acute Acidosis	Chronic Acidosis				
Heat shock protein HSP 90-beta	P34058	Hsp90ab1	-	-	1	TKPIWTRNPDDITQEEYGEFYK	K286	No	Yes
Sorbitol dehydrogenase	P27867	Sord	1	1	1	AAPAKGENLSLVVHGPGDIR	K6	No	No
Transitional endoplasmic reticulum ATPase	P46462	Vcp	-	3	-	ASGADSKGDDLSTAILK	K8	Yes	No
40S ribosomal protein S24	D4A6H5	Rps24	-	1	-	QMVIDVLHPGKATVPK	K32	Yes	Yes
Similar to RIKEN cDNA C630028N24 gene (Predicted), isoform CRA_b	D3ZUX1	Agphd1	-	4	-	SSGDDQQSQAFTKPTFTEAQASALVESIFGFK	K14	No	No
Uncharacterized protein	F1LNM3	Ank3	1	-	1	DPSKELAGLFEHK	K2224	No	Yes
14-3-3 protein zeta/delta	P63102	Ywhaz	-	1	-	NLLSVAYKNVVGAR	K49	Yes	No
Aldo-keto reductase family 1, member C1	Q3MHS3	Akr1c1	1	-	-	GVVVLAKSFTEKR	K275	Yes	No
Acyl-CoA-binding protein	P11030	Dbi	-	1	-	ENAMKTYVEKVEELK	K72 or K77	No	No
Cytoplasmic dynein 1 heavy chain 1	P38650	Dync1h1	-	1	-	VQSKVNLK	K1113	Yes	Yes
Uncharacterized protein	D4A5F2	Cep290	5	4	5	KNILLEEKLNK	K2445	Yes	Yes
Uncharacterized protein	D3Z8J0	RGD1564425	-	1	-	KLKAQMD	K199	No	Yes
Uncharacterized protein	F1LP82	Rab2a	1	-	1	MITIDGKQIK	K53	Yes	Yes
26S protease regulatory subunit 4	P62193	Psmc1	-	-	1	TLLAKAVANQTSATFLR	K237	No	Yes
RCG21481, isoform CRA_b	D3ZLD5	Golga3	1	1	-	DKFMLQAKVSELK	K1308	Yes	Yes

* If no site determining ions were detected, all possible modification sites are listed. Trypsin does not cleave after an acetylated lyisne. Thus, a single internal lysine must be the sight of modification for peptides with a single internal lysine, and no site determining ion.

PCT as a whole responds to MA, we have combined the cytosolic data from this study with the previously reported data. All proteins found to be differentially expressed at any stage of MA, in any of the subcellular enrichments, were combined to perform these analyses. The previous study of isolated brush border membrane vesicles (44) suggested that a small fraction of the enzymes of glycolysis associate with the apical membrane during normal acid-base balance, but dissociate during acidosis. None of these enzymes were found to be differentially expressed in the cytosolic fractions where the majority of these proteins reside. Therefore, it is likely that the changes observed in the apical membrane were not representative of differences in cellular concentration, so these proteins were excluded from the remainder of the analyses. In total, 141 proteins were found to be differentially regulated across all three datasets, of which 92 were up regulated, 45 were down regulated, and 4 were found to be both up regulated and down regulated at different stages of acidosis.

In order to elucidate which cellular pathways were affected by acidosis, the altered proteins were grouped into the general categories of increasing and decreasing, regardless of the time point at which the change was observed. The gene names for all of the proteins in each of these groups were separately submitted to the web-based STRING protein interaction network tool (http://www.string-db.org) (39). All of the settings in the software were kept at their default parameters with the exception that text mining based associations were omitted. The resulting interaction maps for the increasing and decreasing proteins are shown in Figures 5 and 6, respectively. In these figures, each individual protein is represented as a colored dot, with predicted interactions represented by blue lines. The thickness of the line correlates to the amount of evidence suggesting the association, where the thicker lines are supported by more evidence than the thinner ones. Often, clusters of interconnected proteins are representative of a

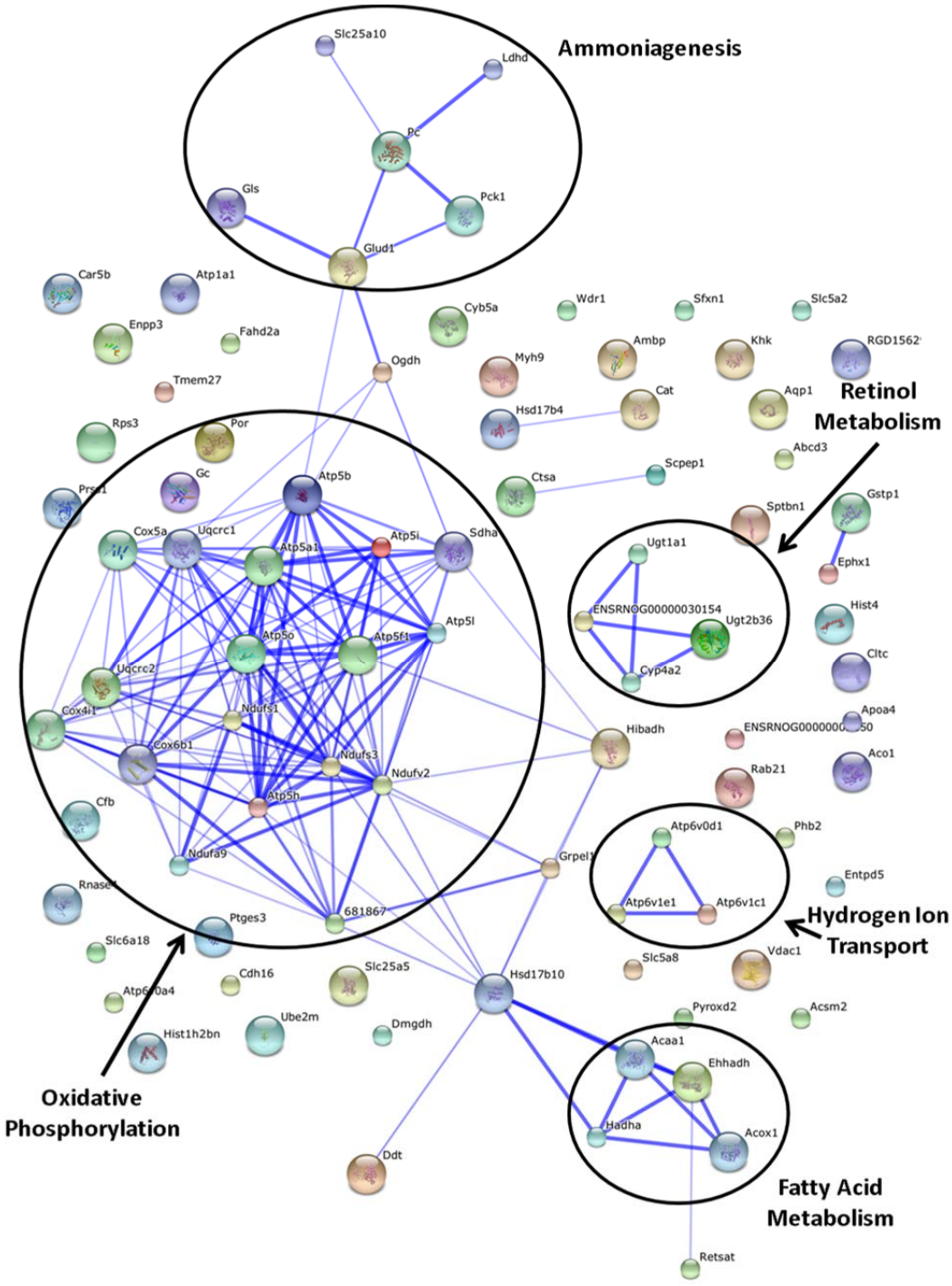

Fig. 5. STRING pathway analysis of proteins that are increased in the PCT at any time time point during acidosis. MS data collected from the cytosolic, mitochondrial (11) , and apical membrane (44) studies were included for this analysis. Thicker lines are indicative of higher evidence of association. All proteins are labeled by their gene name.

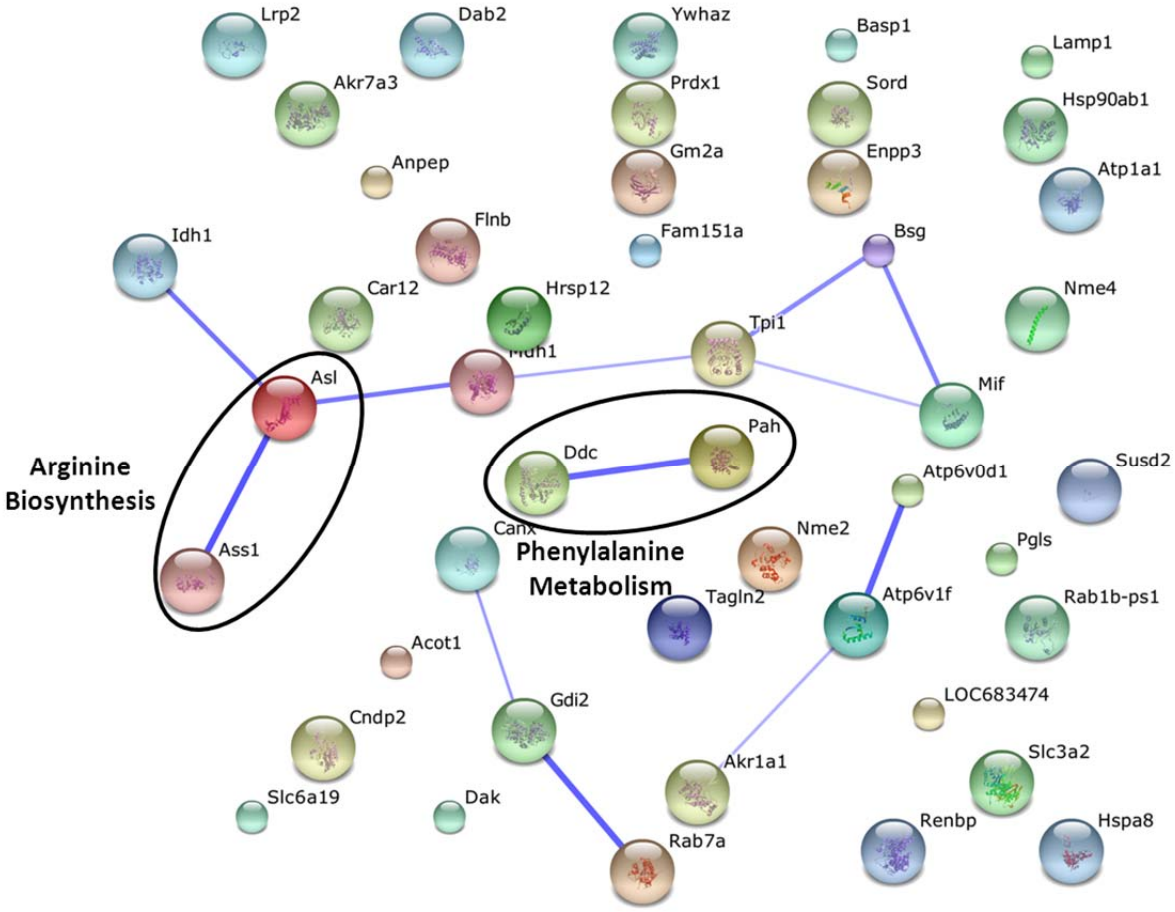

Fig. 6. STRING pathway analysis of all decreasing proteins. Data from cytosolic, mitochondrial (11) and apical membrane (44) analyses were pooled. Individual proteins are labeled by gene name and thicker lines represent more evidence of association.

particular cellular process or pathway. In the map of increasing proteins (Fig. 5), several such clusters are evident, with the most prominent one indicative of oxidative phosphorylation. The other up-regulated processes that are evident in the STRING output include ammoniagenesis, retinol metabolism, hydrogen ion transport, and fatty acid metabolism. A few small clusters were present in the analysis of the decreasing proteins, but they contained only a few proteins (Fig. 6). Identifiable clusters contain proteins involved in arginine biosynthesis and phenylalanine metabolism

In addition to the STRING analysis, each protein in the combined list was manually annotated with a single cellular process or function. Manual assignment of such functions was used because proteins are often annotated with multiple GO terms or KEGG pathways, making it difficult to select a single annotation for each protein. With the manual assignments, related categories were combined to group the proteins into broad categories. Pie charts showing the percentage of the increasing proteins belonging to each of the broad cellular processes are presented in Figure 7A, where the decreasing proteins are shown in Figure 7B. In concurrence with the STRING annotations, 18% of the increasing proteins could be grouped into the category of oxidative phosphorylation (Fig. 7A). Many of the other proteins found to be increasing were related to lipid metabolism (10%), amino acid metabolism (5%), ion transport (4%), and carbohydrate metabolism (4%). For the down-regulated proteins, many were involved in amino acid (14%), carbohydrate (12%), and lipid metabolism (8%). Other annotated processes include ion transport, protein folding, and cellular signaling.

Finally, KEGG annotations and GO term biological processes were compiled from STRING for all of the differentially regulated proteins. A subset of the resulting annotations was compared in order to visualize the number of proteins that were found to be increasing or

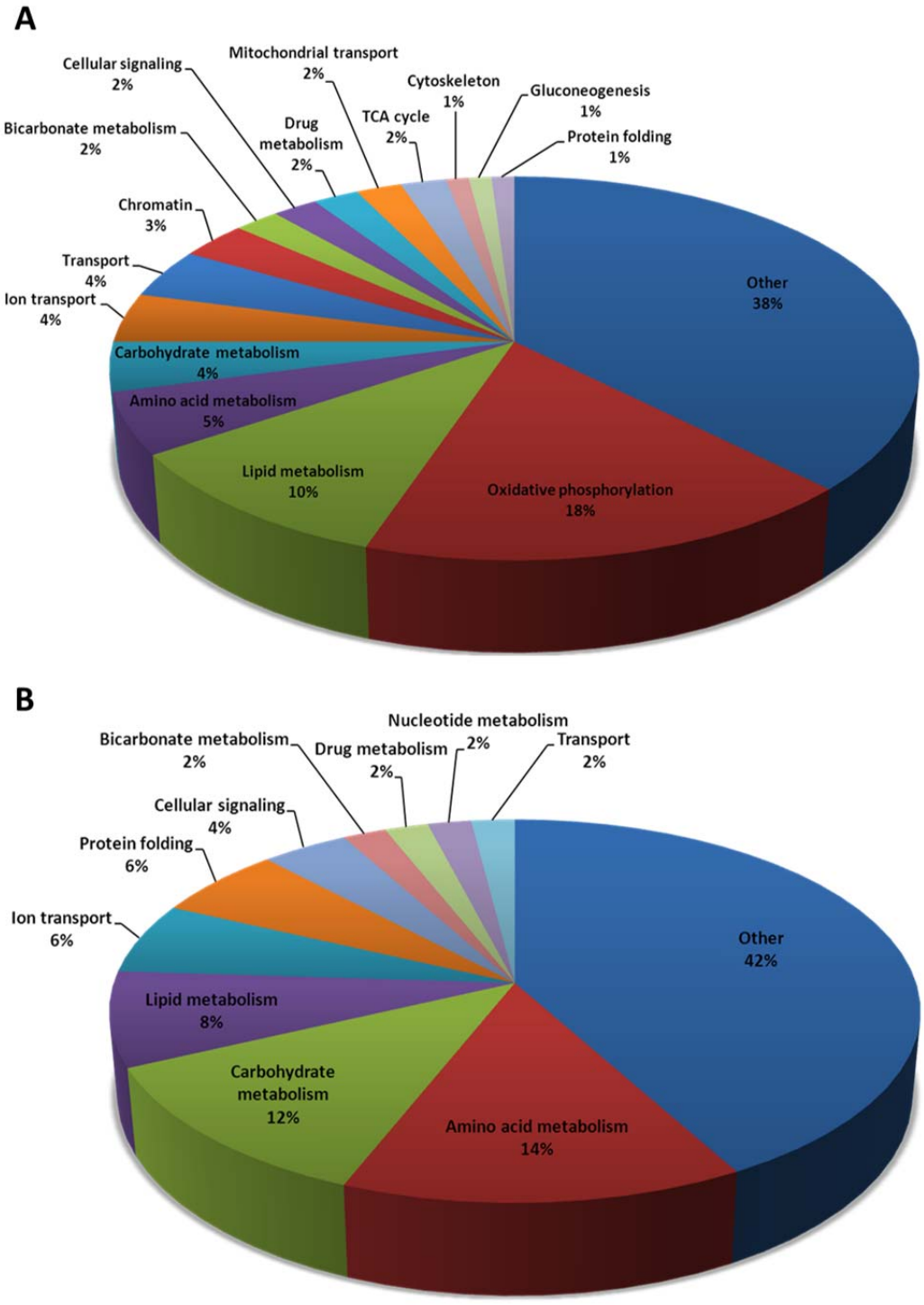

Fig. 7. Cellular functions for all proteins found to be differentially regulated at any stage of metabolic acidosis. Data from cytosolic, mitochondrial (11), and apical membrane (44) fractions were combined and functions were manually assigned for all proteins. **A)** Proteins identified by MS analysis as being up regulated during metabolic acidosis. **B)** Down regulated proteins in acidosis.

decreasing for each annotation (Fig. 8). As was suggested by both the STRING output and the manually annotated pie charts, many proteins involved in oxidative phosphorylation were found to be increasing across all of the datasets, but very few were decreasing. Other processes that were annotated with a number of up-regulated proteins, but few down-regulated included proximal convoluted tubule bicarbonate reclamation, TCA cycle, fatty acid metabolism, retinol metabolism, metabolism of xenobiotics, nitrogen metabolism, nucleotide metabolism, ion transport and proton transport. Interestingly, relatively few pathways contained primarily down-regulated proteins.

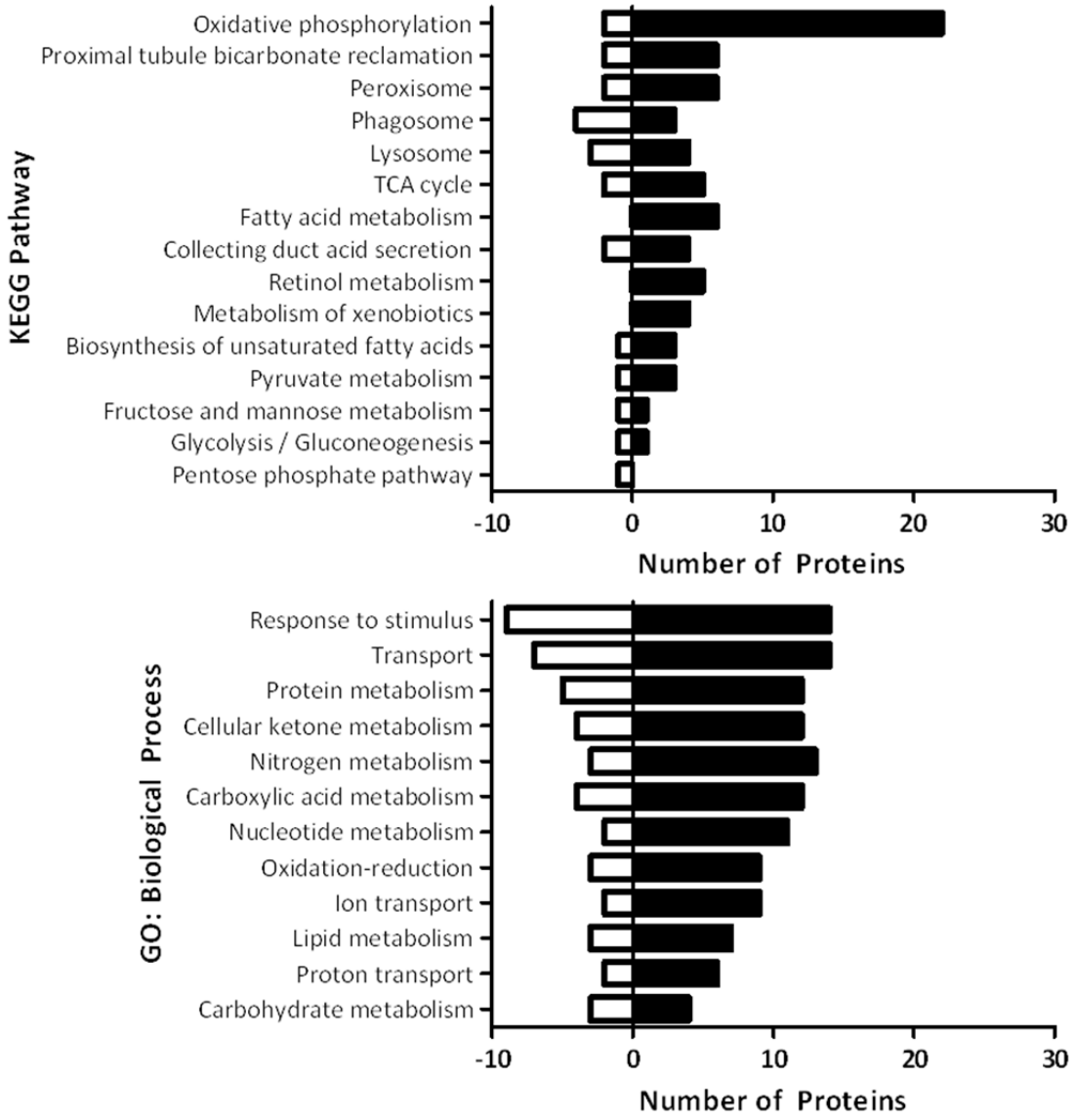

Fig. 8. A subset of the pathways and biological processes found to be up or down regulated during metabolic acidosis. Black bars to the right of the x-axis represent the number of proteins involved in the pathway or process that were up regulated during acidosis, where white bars to the left of the axis represent the number of down regulated proteins. Data from cytosolic, mitochondrial (11) and apical membrane (44) fractions were concatenated prior to analysis.

DISCUSSION

A variety of proteins that reside in the cytosol are known to contribute to the response of the PCT to metabolic acidosis. It has been well established that the onset of acidosis triggers the uptake of plasma glutamine in the PCT, followed by increased glutamine catabolism and gluconeogenesis (6). The increased conversion of glutamine to glucose also results in the net production of bicarbonate ions that are transported into the blood to help restore acid-base homeostasis (6). Although glutamine uptake and metabolism is dependent upon apical and basolateral transporters and mitochondrial proteins, respectively, the process of gluconeogenesis occurs in the cytoplasm. The increase in gluconeogenesis is due, at least in part, to the increased synthesis of cytosolic phosphoenolpyruvate carboxykinase (PEPCK), which occurs via an increased rate of transcription as well as stabilization of the PCK mRNA (16, 19, 29). Although the role of gluconeogenesis in the PCT response to acidosis has been well established, the effects of acidosis on other cellular processes that occur in the cytoplasm remain to be elucidated. This study presents the first comprehensive analysis of the proteome of the cytosolic fraction of the PCT and its response to MA. These data, when combined with other proteomics data (11, 44), increases our knowledge of the overall cellular response of the PCT to MA.

In accordance with previous work, PEPCK was significantly increased in acidotic samples as compared to controls (7). This increase plays an important role in the up-regulation of gluconeogenesis and bicarbonate production that helps to restore acid-base homeostasis. Other proteins including low-density lipoprotein receptor-related protein 2, N-acylglucosamine 2-epimerase, aromatic-L-amino-acid decarboxylase, and phenylalanine-4-hydroxylase exhibit changes in protein levels during the onset of acidosis that closely correlate with changes in their mRNAs, as was previously observed by microarray analysis of the mouse kidney transcriptome

(32). In addition, the observed changes in glutathione S-transferase P and pyruvate carboxylase also agree with the results of the previous difference gel electrophoresis (DIGE) analysis of isolated rat PCT (7). Surprisingly, peptides from the low-density lipoprotein receptor related protein-2 (megalin) and the alpha subunit of the Na^+/K^+-ATPase (AT1A1), which are very abundant integral proteins of the apical and basolateral membranes, respectively, were identified in the cytosolic fractions. The observation of these proteins may be associated with small vesicles or endosomes that were not removed by the high-speed centrifugation step. Interestingly, the 7 to 10-fold decrease observed for AT1A1 in the cytosolic fraction disagrees with the 1.5 to 2-fold increase previously observed in the analysis of isolated brush border membrane vesicles (44). Thus, it is possible that more of the AT1A1 protein is sequestered in cytoplasmic vesicles during normal acid-base balance and then moved to the plasma membrane during acidosis.

Although a number of the differentially regulated proteins observed in this study were previously described, 15 of the 24 responding proteins are novel. Transgelin-2, an actin-binding protein that plays a role in the regulation of angiogenesis (46), was found to decrease greater than 2-fold during chronic acidosis. Previous data suggests that transgelin-2 inhibits endothelial migration and tube formation *in vivo* (46). Hence, the observed down-regulation of this protein may be representative of increased angiogenesis. Although angiogenesis is necessary for proper maintenance of renal tissue, it has also been implicated in the progression of chronic kidney disease (25, 27). This information combined with the renal hypertrophy and increased glutamine extraction suggests that there may be an increase in renal angiogenesis occurring during chronic acidosis.

Prostaglandin E synthase 3 was a protein found to be up regulated in the acidotic samples that has not been previously associated with the condition. PTGES3 is a molecular chaperone that aides in transcription activation by the disassembly of transcriptional regulatory complexes in response to hormone stimulation (9). Although this method of transcriptional regulation has not been previously associated with acidosis, it is possible that the greater than 3.5 fold increase in this protein contributes to some of the other changes in protein abundance that occur in the PCT during MA.

The increase in the cytoplasmic isoform of aconitase (ACO1) was another novel change. Cytoplasmic citrate can be converted to isocitrate by ACO1, which is then converted to α-ketogluterate by the $NADP^+$-dependent isocitrate dehydrogenase enzyme (42). This reaction reduces $NADP^+$ to NADPH, which is an important cofactor in fatty acid metabolism (42). The up-regulation of the ACO1 enzyme may be representative of the need to increase NADPH production. In addition, previous work has found the mitochondrial isoform of this protein increases in both abundance and activity during acidosis (7, 28), which leads to an increased rate of isocitrate synthesis in the mitochondria as part of the TCA cycle. It is possible that the excess isocitrate produced in the cytosol by ACO1 could be transported into the mitochondria via known isocitrate transporters (14) and enter the TCA cycle. Other cytosolic proteins, which exhibit novel changes during acidosis, function in actin disassembly, carbohydrate metabolism, immune response, protein translation and lipid metabolism among others, but the roles of these proteins in the acidotic response is uncertain.

Previous work has established that mRNA stabilization is responsible for the differential expression observed for several PCT proteins during MA (20, 29, 35). These proteins include PEPCK, glutaminase and glutamine dehydrogenase, all of which contain one or two 8-

nucleotide, AU-rich elements in the 3'-untranslated region that function as pH responsive elements (pHREs) (29, 35). Interestingly, 6 of the 14 cytosolic proteins found in our study to be increased in acidosis contain at least one AU-rich sequence with 85% sequence homology to a pHRE, suggesting these proteins may be increased due to mRNA stabilization. Further investigation is necessary to determine if this mode of regulation is actually occurring in these proteins.

In recent years, the role of lysine acetylation in non-histone proteins has become more apparent (2, 15, 47). However, much work is still needed to fully understand the impact of this modification on cellular processes. Previous work has suggested that lysine acetylation of mitochondrial proteins in the PCT may play a role in acid-base homeostasis (11). Therefore, we sought to determine which cytosolic proteins of the PCT undergo lysine acetylation. It is important to note, however, that due to the limited mass accuracy and mass range limitations of the linear ion trap mass spectrometer used in this study, it was not feasible to distinguish between lysine acetylation and trimethylation which have nearly identical masses. Most of the work to date has found that trimethyl lysine modifications are commonly found only in the nucleus, suggesting that the majority of modifications discovered on the cytosolic protein are indeed acetylation events (2, 18). Interestingly, only 15 unique peptides with acetylated lysines were identified in this analysis, with no more than five modified peptides present for a single protein in a treatment (Table 1). This is quite different from the results of a similar analysis of acetylation in PCT mitochondrial proteins where > 20 spectra of the same modified peptide were regularly identified in control or chronically acidotic samples (11). Previous work has established that PEPCK stability is decreased by the acetylation of three specific lysine residues, and that higher concentrations of amino acids can lead to decreased acetylation and increased

stability of PEPCK (47). Due to the increased rate of glutamine uptake in the PCT during acidosis, we hypothesized that little to no acetylation of PEPCK would be observed, which was indeed the case. However, PEPCK acetylation was also not observed in the control group, suggesting that perhaps this method of regulation is not as prominent in the PCT. Overall, due to the low number of total acetylated peptides identified during the MS analysis, it appears that lysine acetylation may play a minor role in the regulation of cytosolic proteins in the PCT during MA.

Using just the cytosolic protein data collected here, it is difficult to determine which cellular pathways are affected by MA. However, when the data are combined with previous proteomic characterizations of apical membrane (44) and mitochondrial (11) proteins, several trends begin to appear. STRING analysis revealed several large clusters that are indicative of activated cellular processes (Fig. 5 & 6). By far the largest such grouping is comprised of proteins related to oxidative phosphorylation (Fig. 5). As expected, the majority of these proteins were identified in mitochondria (11). It is likely that this up regulation of cellular ATP production is necessary to keep up with the increased glutamine catabolism and energy demands in the cell. The extensive remodeling of the cellular proteome associated with the increase in glutamine uptake, catabolism and gluconeogenesis, produce hypertrophy that increases the energy demands on the cell. Other increased cellular processes identified by STRING analysis include hydrogen ion transport, as well as retinol, pyruvate and fatty acid metabolism (Fig. 5). The increase in hydrogen ion transport is expected during acidosis, due to the increased rate of hydrogen ion secretion into the tubular lumen. The increase in pyruvate production is likely closely coupled to the increase in gluconeogenesis in the PCT, since pyruvate is an additional starting material for this pathway. Interestingly, renal disease associated with diabetes causes a

dysregulation of retinol metabolism in the renal cortex (18). Thus the observed regulation of retinol may be generally associated with cellular stress in the kidneys. It has been well established that retinol (vitamin A) plays an important role in epithelium maintenance (4), thus, it is probable that the maintenance of the renal epithelium is associated with the observed changes in retinol metabolism. Further investigation is necessary to pursue this hypothesis. The observed increase in proteins involved in fatty acid metabolism is also correlated with the expected increase in NADPH production in the cytosol, described above. Several enzymes involved in fatty acid metabolism require NADPH as a cofactor (24), thus, an increase in fatty acid production would require an increase in available NADPH. The number of proteins found to decrease in response to acidosis is less than the number that increase. As a result, the STRING analysis of this group of proteins did not identify significant clusters of proteins (Fig. 6).

Our proteome characterization of the cytosolic subfraction of the PCT, combined with previously reported characterization of the apical membrane and mitochondrial subcellular fractions have enabled a comprehensive analysis of the response of the PCT proteome to MA (11, 44). Taken together, the data presented here suggests that several cellular pathways in the PCT seem to be affected by MA, however, further research is necessary to better understand the physiology and responsible mechanisms of the observed changes.

REFERENCES

1. Normalizing Spectral Counts in Scaffold Proteome Software. http://www.proteomesoftware.com/pdf_files/Normalizing_Spectral_Counting-Scaffold.pdf. [December 9, 2012].

2. **Arif M, Selvi BR, and Kundu TK**. Lysine acetylation: the tale of a modification from transcription regulation to metabolism. *Chembiochem : a European journal of chemical biology* 11: 1501-1504, 2010.

3. **Asara JM, Christofk HR, Freimark LM, and Cantley LC**. A label-free quantification method by MS/MS TIC compared to SILAC and spectral counting in a proteomics screen. *PROTEOMICS* 8: 994-999, 2008.

4. **Blomhoff R, and Blomhoff HK**. Overview of retinoid metabolism and function. *Journal of neurobiology* 66: 606-630, 2006.

5. **Charles J, and Heilman R**. Metabolic Acidosis. *Hospital Physician* 41: 37-42, 2005.

6. **Curthoys NP, and Gstraunthaler G**. Mechanism of increased renal gene expression during metabolic acidosis. *American journal of physiology Renal physiology* 281: F381-390, 2001.

7. **Curthoys NP, Taylor L, Hoffert JD, and Knepper MA**. Proteomic analysis of the adaptive response of rat renal proximal tubules to metabolic acidosis. *American journal of physiology Renal physiology* 292: F140-147, 2007.

8. **Elias JE, and Gygi SP**. Target-decoy search strategy for mass spectrometry-based proteomics. *Methods Mol Biol* 604: 55-71, 2010.

9. **Freeman BC, and Yamamoto KR**. Disassembly of transcriptional regulatory complexes by molecular chaperones. *Science* 296: 2232-2235, 2002.

10. **Freund DM, and Prenni JE**. Improved Detection of Quantitative Differences Using a Combination of Spectral Counting and MS/MS Total Ion Current. *J Proteome Res* 2013.

11. **Freund DM, Prenni JE, and Curthoys NP**. Response of the mitochondrial proteome of rat renal proximal convoluted tubules to chronic metabolic acidosis. *Am J Physiol Renal Physiol* 304: F145-155, 2013.

12. **Ghazalpour A, Bennett B, Petyuk VA, Orozco L, Hagopian R, Mungrue IN, Farber CR, Sinsheimer J, Kang HM, Furlotte N, Park CC, Wen PZ, Brewer H, Weitz K, Camp DG, 2nd, Pan C, Yordanova R, Neuhaus I, Tilford C, Siemers N, Gargalovic P, Eskin E, Kirchgessner T, Smith DJ, Smith RD, and Lusis AJ**. Comparative analysis of proteome and transcriptome variation in mouse. *PLoS genetics* 7: e1001393, 2011.

13. **Gilany K, Moens L, and Dewilde S**. Mass spectrometry-based proteomics in the life sciences: a review. *Journal of Paramedical Sciences* 1: 53-78, 2010.

14. **Gnoni GV, Priore P, Geelen MJ, and Siculella L**. The mitochondrial citrate carrier: metabolic role and regulation of its activity and expression. *IUBMB life* 61: 987-994, 2009.

15. **Guarente L**. The logic linking protein acetylation and metabolism. *Cell Metab* 14: 151-153, 2011.

16. **Gummadi L, Taylor L, and Curthoys NP**. Concurrent binding and modifications of AUF1 and HuR mediate the pH-responsive stabilization of phosphoenolpyruvate carboxykinase mRNA in kidney cells. *Am J Physiol Renal Physiol* 303: F1545-1554, 2012.

17. **Huling JC, Pisitkun T, Song JH, Yu M-J, Hoffert JD, and Knepper MA**. Gene Expression Databases for Kidney Epithelial Cells. *AJP: Renal Physiology* 2011.

18. **Huq MD, Tsai NP, Khan SA, and Wei LN**. Lysine trimethylation of retinoic acid receptor-alpha: a novel means to regulate receptor function. *Molecular & cellular proteomics : MCP* 6: 677-688, 2007.

19. **Hwang JJ, and Curthoys NP**. Effect of acute alterations in acid-base balance on rat renal glutaminase and phosphoenolpyruvate carboxykinase gene expression. *J Biol Chem* 266: 9392-9396, 1991.

20. **Hwang JJ, Perera S, Shapiro RA, and Curthoys NP**. Mechanism of altered renal glutaminase gene expression in response to chronic acidosis. *Biochemistry* 30: 7522-7526, 1991.

21. **Janech MG, Raymond JR, and Arthur JM**. Proteomics in renal research. *AJP: Renal Physiology* 292: F501-F512, 2006.

22. **Keller A, Nesvizhskii AI, Kolker E, and Aebersold R**. Empirical statistical model to estimate the accuracy of peptide identifications made by MS/MS and database search. *Anal Chem* 74: 5383-5392, 2002.

23. **Knepper MA**. Proteomics and the Kidney. *Journal of the American Society of Nephrology* 13: 1398-1408, 2002.

24. **Koh HJ, Lee SM, Son BG, Lee SH, Ryoo ZY, Chang KT, Park JW, Park DC, Song BJ, Veech RL, Song H, and Huh TL**. Cytosolic NADP+-dependent isocitrate dehydrogenase plays a key role in lipid metabolism. *J Biol Chem* 279: 39968-39974, 2004.

25. **Lerman LO, and Chade AR**. Angiogenesis in the kidney: a new therapeutic target? *Curr Opin Nephrol Hypertens* 18: 160-165, 2009.

26. **Lotspeich WD**. Renal Hypertrophy in Metabolic Acidosis and Its Relation to Ammonia Excretion. *The American journal of physiology* 208: 1135-1142, 1965.

27. **Maeshima Y, and Makino H**. Angiogenesis and chronic kidney disease. *Fibrogenesis & tissue repair* 3: 13, 2010.

28. **Melnick JZ, Preisig PA, Moe OW, Srere P, and Alpern RJ**. Renal cortical mitochondrial aconitase is regulated in hypo- and hypercitraturia. *Kidney international* 54: 160-165, 1998.

29. **Mufti J, Hajarnis S, Shepardson K, Gummadi L, Taylor L, and Curthoys NP**. Role of AUF1 and HuR in the pH-responsive stabilization of phosphoenolpyruvate carboxykinase mRNA in LLC-PK(1)-F(+) cells. *Am J Physiol Renal Physiol* 301: F1066-1077, 2011.

30. **Nesvizhskii AI, Keller A, Kolker E, and Aebersold R**. A statistical model for identifying proteins by tandem mass spectrometry. *Anal Chem* 75: 4646-4658, 2003.

31. **Nikolov M, Schmidt C, and Urlaub H**. Quantitative mass spectrometry-based proteomics: an overview. *Methods Mol Biol* 893: 85-100, 2012.

32. **Nowik M, Lecca MR, Velic A, Rehrauer H, Brändli AW, and Wagner CA**. Genome-wide gene expression profiling reveals renal genes regulated during metabolic acidosis. *Physiological genomics* 32: 322-334, 2008.

33. **Oberg AL, Mahoney DW, Eckel-Passow JE, Malone CJ, Wolfinger RD, Hill EG, Cooper LT, Onuma OK, Spiro C, Therneau TM, and Bergen III HR**. Statistical Analysis of Relative Labeled Mass Spectrometry Data from Complex Samples Using ANOVA. *Journal of proteome research* 7: 225-233, 2008.

34. **Pfaller W, Seppi T, Ohno A, Giebisch G, and Beck FX**. Quantitative morphology of renal cortical structures during compensatory hypertrophy. *Experimental nephrology* 6: 308-319, 1998.

35. **Schroeder JM, Liu W, and Curthoys NP**. pH-responsive stabilization of glutamate dehydrogenase mRNA in LLC-PK1-F+ cells. *American journal of physiology Renal physiology* 285: F258-265, 2003.

36. **Shechter P, Shi JD, and Rabkin R**. Renal tubular cell protein breakdown in uninephrectomized and ammonium chloride-loaded rats. *Journal of the American Society of Nephrology : JASN* 5: 1201-1207, 1994.

37. **Silbernagl S**. Tubular reabsorption of L-glutamine studied by free-flow micropuncture and microperfusion of rat kidney. *The International journal of biochemistry* 12: 9-16, 1980.

38. **Smith PK, Krohn RI, Hermanson GT, Mallia AK, Gartner FH, Provenzano MD, Fujimoto EK, Goeke NM, Olson BJ, and Klenk DC**. Measurement of Protein Using Bicinchoninic Acid. *Anal Biochem* 150: 76-85, 1985.

39. **Szklarczyk D, Franceschini A, Kuhn M, Simonovic M, Roth A, Minguez P, Doerks T, Stark M, Muller J, Bork P, Jensen LJ, and von Mering C**. The STRING database in 2011: functional interaction networks of proteins, globally integrated and scored. *Nucleic acids research* 39: D561-568, 2011.

40. **Tang A, and Curthoys NP**. Identification of zeta-crystallin/NADPH:quinone reductase as a renal glutaminase mRNA pH response element-binding protein. *J Biol Chem* 276: 21375-21380, 2001.

41. **Taverner T, Karpievitch YV, Polpitiya AD, Brown JN, Dabney AR, Anderson GA, and Smith RD**. DanteR: an extensible R-based tool for quantitative analysis of -omics data. *Bioinformatics* 28: 2404-2406, 2012.

42. **Tong WH, and Rouault TA**. Metabolic regulation of citrate and iron by aconitases: role of iron-sulfur cluster biogenesis. *Biometals : an international journal on the role of metal ions in biology, biochemistry, and medicine* 20: 549-564, 2007.

43. **Walmsley SJ, Broeckling C, Hess A, Prenni J, and Curthoys NP**. Proteomic analysis of brush-border membrane vesicles isolated from purified proximal convoluted tubules. *American journal of physiology Renal physiology* 298: F1323-1331, 2010.

44. **Walmsley SJ, Freund DM, and Curthoys NP**. Proteomic profiling of the effect of metabolic acidosis on the apical membrane of the proximal convoluted tubule. *AJP: Renal Physiology* 302: F1465-1477, 2012.

45. **Weiner ID, and Hamm LL**. Molecular mechanisms of renal ammonia transport. *Annual review of physiology* 69: 317-340, 2007.

46. **Xiao Y, Li Y, Han J, Pan Y, Tie L, and Li X**. Transgelin 2 participates in lovastatin-induced anti-angiogenic effects in endothelial cells through a phosphorylated myosin light chain-related mechanism. *PLoS ONE* 7: e46510, 2012.

47. **Zhao S, Xu W, Jiang W, Yu W, Lin Y, Zhang T, Yao J, Zhou L, Zeng Y, Li H, Li Y, Shi J, An W, Hancock SM, He F, Qin L, Chin J, Yang P, Chen X, Lei Q, Xiong Y, and Guan KL**. Regulation of cellular metabolism by protein lysine acetylation. *Science* 327: 1000-1004, 2010.

48. **Zhu W, Smith JW, and Huang C-M**. Mass Spectrometry-Based Label-Free Quantitative Proteomics. *Journal of Biomedicine and Biotechnology* 2010: 1-7, 2010.

APPENDIX I

Table 4: All proteins identified by mass spectrometry analysis

Protein Name	UniProt Entry Name	UniProt Accession	Gene Name	Molecular Weight	Mean Spectral Counts ± SEM		
					Control	1 Day	7 Day
Hydroxyacid oxidase 2	HAOX2_RAT	Q07523	Hao2	39 kDa	735.0 ± 141.6	1001.0 ± 178.2	778.0 ± 87.2
Alpha-enolase	ENOA_RAT	P04764	Eno1	47 kDa	562.7 ± 184.8	671.3 ± 151.2	466.7 ± 62.1
Fructose-bisphosphate aldolase	Q66HT1_RAT	Q66HT1	Aldob	40 kDa	457.0 ± 65.3	446.3 ± 47.5	559.7 ± 26.2
Uncharacterized protein	D4AD25_RAT	D4AD25	Cltc	192 kDa	309.3 ± 77.8	491.3 ± 59.5	389.3 ± 56.3
Fructose-1,6-bisphosphatase 1	F16P1_RAT	P19112	Fbp1	40 kDa	376.3 ± 90.6	417.3 ± 51.2	360.0 ± 23.0
Phosphoenolpyruvate carboxykinase, cytosolic [GTP]	PCKGC_RAT	P07379	Pck1	69 kDa	107.3 ± 23.1	644.3 ± 13.6	344.3 ± 55.8
Actin, cytoplasmic 2	ACTG_RAT	P63259	Actg1	42 kDa	303.0 ± 41.8	300.7 ± 41.3	243.3 ± 22.9
Tubulin beta-4B chain	TBB4B_RAT	Q6P9T8	Tubb4b	50 kDa	271.3 ± 40.7	303.3 ± 16.2	230.7 ± 3.8
Glyceraldehyde-3-phosphate dehydrogenase	D3ZGY4_RAT	D3ZGY4	Gapdh-ps2	36 kDa	276.7 ± 16.0	273.3 ± 29.9	240.3 ± 43.0
Tubulin beta-5 chain	TBB5_RAT	P69897	Tubb5	50 kDa	250.7 ± 40.1	267.0 ± 32.1	223.7 ± 17.8
Major urinary protein	MUP_RAT	P02761	N/A	21 kDa	328.0 ± 152.5	99.7 ± 27.9	249.7 ± 136.9
Tubulin alpha-1C chain	TBA1C_RAT	Q6AYZ1	Tuba1c	50 kDa	189.0 ± 64.0	254.3 ± 55.1	211.0 ± 39.1
Tubulin alpha-4A chain	TBA4A_RAT	Q5XIF6	Tuba4a	50 kDa	181.7 ± 60.7	237.3 ± 51.8	195.7 ± 43.0
Glutathione S-transferase alpha-1	GSTA1_RAT	P00502	Gsta1	26 kDa	200.0 ± 29.1	213.0 ± 8.0	201.7 ± 42.2
Uncharacterized protein	D3ZXY4_RAT	D3ZXY4	Aldh8a1	53 kDa	202.0 ± 26.9	211.0 ± 18.0	184.7 ± 12.8
Tubulin beta-2A chain	TBB2A_RAT	P85108	Tubb2a	50 kDa	247.0 ± 38.6	187.0 ± 93.6	153.3 ± 76.7
Glutathione S-transferase alpha-3	GSTA3_RAT	P04904	Gsta3	25 kDa	157.0 ± 52.5	216.7 ± 52.1	197.3 ± 73.7
Malate dehydrogenase, cytoplasmic	MDHC_RAT	O88989	Mdh1	36 kDa	159.3 ± 63.8	225.7 ± 60.7	147.7 ± 29.6
Catalase	CATA_RAT	P04762	Cat	60 kDa	129.7 ± 20.2	195.0 ± 31.5	163.3 ± 20.3
Argininosuccinate synthase	ASSY_RAT	P09034	Ass1	46 kDa	155.0 ± 36.8	181.0 ± 32.3	147.7 ± 15.6
Alcohol dehydrogenase [NADP+]	AK1A1_RAT	P51635	Akr1a1	37 kDa	179.7 ± 74.7	132.3 ± 24.5	115.7 ± 42.1
Transketolase, isoform CRA_a	G3V826_RAT	G3V826	Tkt	71 kDa	104.3 ± 12.8	119.7 ± 6.1	118.0 ± 36.2
Heat shock protein HSP 90-beta	HS90B_RAT	P34058	Hsp90ab1	83 kDa	90.0 ± 18.8	136.0 ± 18.4	109.3 ± 19.4
Aflatoxin B1 aldehyde reductase member 3	ARK73_RAT	P38918	Akr7a3	37 kDa	117.0 ± 22.6	98.3 ± 36.1	107.7 ± 13.0
Isocitrate dehydrogenase [NADP] cytoplasmic	IDHC_RAT	P41562	Idh1	47 kDa	103.0 ± 49.7	101.7 ± 17.7	63.7 ± 8.7
Actin, alpha cardiac muscle 1	ACTC_RAT	P68035	Actc1	42 kDa	100.7 ± 21.8	88.3 ± 6.7	67.0 ± 6.6
Heat shock protein HSP 90-alpha	HS90A_RAT	P82995	Hsp90aa1	85 kDa	66.3 ± 23.4	92.7 ± 20.3	91.0 ± 15.6
Heat shock cognate 71 kDa protein	HSP7C_RAT	P63018	Hspa8	71 kDa	78.3 ± 26.5	105.3 ± 39.6	59.0 ± 7.0
L-lactate dehydrogenase B chain	LDHB_RAT	P42123	Ldhb	37 kDa	73.7 ± 15.2	97.3 ± 36.5	67.7 ± 10.3

Protein Name	UniProt Entry Name	UniProt Accession	Gene Name	Molecular Weight	Mean Spectral Counts ± SEM		
					Control	1 Day	7 Day
Tubulin, beta 6	Q4QQV0_RAT	Q4QQV0	Tubb6	50 kDa	86.3 ± 14.4	79.7 ± 45.6	70.3 ± 36.8
Retinal dehydrogenase 1	AL1A1_RAT	P51647	Aldh1a1	54 kDa	62.0 ± 8.5	102.3 ± 14.8	61.7 ± 17.2
Elongation factor 1-alpha	D3ZC88_RAT	D3ZC88	LOC100360413	50 kDa	65.3 ± 12.3	70.0 ± 11.7	75.0 ± 11.2
Uncharacterized protein	B5DFA0_RAT	B5DFA0	Vil1	93 kDa	58.0 ± 12.1	93.7 ± 8.5	54.3 ± 2.0
Fumarylacetoacetase	FAAA_RAT	P25093	Fah	46 kDa	89.3 ± 37.8	48.3 ± 41.3	66.3 ± 29.7
Rab GDP dissociation inhibitor beta	GDIB_RAT	P50399	Gdi2	51 kDa	69.3 ± 13.8	80.3 ± 11.0	54.0 ± 5.0
Phosphoglycerate kinase 1	PGK1_RAT	P16617	Pgk1	45 kDa	87.0 ± 55.1	69.0 ± 36.8	44.3 ± 14.8
Ribonuclease UK114	UK114_RAT	P52759	Hrsp12	14 kDa	69.3 ± 29.3	40.7 ± 23.1	89.3 ± 36.2
Uncharacterized protein	D4ACL3_RAT	D4ACL3	Aco1	99 kDa	40.0 ± 4.4	102.0 ± 9.3	47.3 ± 9.5
Glucose-6-phosphate isomerase	G6PI_RAT	Q6P6V0	Gpi	63 kDa	57.3 ± 0.9	83.7 ± 13.9	47.0 ± 2.1
Cathepsin B	CATB_RAT	P00787	Ctsb	37 kDa	76.0 ± 27.3	61.7 ± 26.1	48.7 ± 5.9
Sulfotransferase 1C2A	S1C2A_RAT	Q9WUW9	Sult1c2a	35 kDa	76.3 ± 36.3	56.0 ± 14.6	44.7 ± 21.1
Coactosin-like protein	COTL1_RAT	B0BNA5	Cotl1	16 kDa	64.7 ± 9.7	78.3 ± 13.2	32.7 ± 17.0
Bifunctional ATP-dependent dihydroxyacetone kinase/FAD-AMP lyase (cyclizing)	DHAK_RAT	Q4KLZ6	Dak	59 kDa	58.7 ± 16.0	57.3 ± 16.8	59.0 ± 28.5
Threonine synthase-like 2	THNS2_RAT	Q5M7T9	Thnsl2	54 kDa	52.7 ± 7.7	71.0 ± 10.7	47.0 ± 8.5
Superoxide dismutase [Cu-Zn]	SODC_RAT	P07632	Sod1	16 kDa	72.7 ± 40.1	41.7 ± 27.2	55.3 ± 27.0
Uncharacterized protein	F1LNK1_RAT	F1LNK1	Sult1c2	35 kDa	64.0 ± 19.3	56.7 ± 12.3	36.0 ± 14.7
Alpha-actinin-4	ACTN4_RAT	Q9QXQ0	Actn4	105 kDa	57.7 ± 11.7	58.7 ± 12.3	39.3 ± 20.7
Triosephosphate isomerase	TPIS_RAT	P48500	Tpi1	27 kDa	65.3 ± 15.9	57.0 ± 14.6	29.7 ± 5.0
Cofilin-1	COF1_RAT	P45592	Cfl1	19 kDa	54.7 ± 6.9	51.3 ± 6.9	34.0 ± 11.9
Protein NDRG1	NDRG1_RAT	Q6JE36	Ndrg1	43 kDa	37.3 ± 12.3	65.0 ± 26.7	32.0 ± 5.5
4-trimethylaminobutyraldehyde dehydrogenase	AL9A1_RAT	Q9JLJ3	Aldh9a1	54 kDa	29.7 ± 10.0	46.0 ± 21.4	47.0 ± 11.9
Nucleoside diphosphate kinase B	NDKB_RAT	P19804	Nme2	17 kDa	38.3 ± 19.0	51.0 ± 26.1	28.3 ± 3.5
Na(+)/H(+) exchange regulatory cofactor NHE-RF3	NHRF3_RAT	Q9JJ40	Pdzk1	57 kDa	46.7 ± 15.8	50.7 ± 20.3	17.3 ± 7.2
Aldehyde dehydrogenase family 6, subfamily A1, isoform CRA_b	G3V7J0_RAT	G3V7J0	Aldh6a1	58 kDa	26.3 ± 14.7	66.0 ± 15.1	21.3 ± 18.4
Glycine amidinotransferase, mitochondrial	GATM_RAT	P50442	Gatm	48 kDa	27.0 ± 3.2	59.0 ± 12.2	25.7 ± 11.2
Alpha-aminoadipic semialdehyde	AL7A1_RAT	Q64057	Aldh7a1	59 kDa	35.0 ± 2.0	52.0 ± 7.2	24.3 ± 2.4

Protein Name	UniProt Entry Name	UniProt Accession	Gene Name	Molecular Weight	Mean Spectral Counts ± SEM		
					Control	1 Day	7 Day
dehydrogenase							
4-hydroxyphenylpyruvate dioxygenase (Fragment)	F1LNW9_RAT	F1LNW9	Hpd	42 kDa	38.3 ± 9.8	53.7 ± 4.2	16.3 ± 4.4
Transitional endoplasmic reticulum ATPase	TERA_RAT	P46462	Vcp	89 kDa	31.7 ± 12.4	57.3 ± 21.7	18.7 ± 5.0
Protein DJ-1	PARK7_RAT	O88767	Park7	20 kDa	41.7 ± 20.2	34.3 ± 6.1	28.7 ± 9.8
Sorbitol dehydrogenase	DHSO_RAT	P27867	Sord	38 kDa	43.7 ± 9.3	32.3 ± 17.4	28.0 ± 13.0
Isoform A2 of Heterogeneous nuclear ribonucleoproteins A2/B1	ROA2_RAT	A7VJC2	Hnrnpa2b1	36 kDa	23.3 ± 3.8	39.7 ± 19.5	40.7 ± 19.4
Cytosolic non-specific dipeptidase	CNDP2_RAT	Q6Q0N1	Cndp2	53 kDa	45.7 ± 28.2	39.7 ± 13.5	17.7 ± 5.5
Peptidyl-prolyl cis-trans isomerase A	PPIA_RAT	P10111	Ppia	18 kDa	49.3 ± 28.8	33.7 ± 18.6	20.0 ± 6.7
Lambda-crystallin homolog	CRYL1_RAT	Q811X6	Cryl1	35 kDa	25.3 ± 6.2	45.3 ± 3.0	28.7 ± 10.4
Retinoid-inducible serine carboxypeptidase	RISC_RAT	Q920A6	Scpep1	51 kDa	26.7 ± 8.7	56.3 ± 12.1	15.3 ± 4.3
Glycerol-3-phosphate dehydrogenase [NAD+], cytoplasmic	GPDA_RAT	O35077	Gpd1	37 kDa	37.0 ± 16.8	49.7 ± 15.9	9.3 ± 5.4
L-lactate dehydrogenase A chain	LDHA_RAT	P04642	Ldha	36 kDa	31.7 ± 12.5	26.0 ± 12.5	34.3 ± 8.8
Uncharacterized protein (Fragment)	F1M390_RAT	F1M390	Ezr	69 kDa	28.3 ± 3.2	34.0 ± 6.7	28.7 ± 9.7
Aminoacylase-1A	ACY1A_RAT	Q6AYS7	Acy1a	46 kDa	36.3 ± 18.9	32.3 ± 10.2	21.0 ± 3.1
Isoform 2 of Catechol O-methyltransferase	COMT_RAT	P22734	Comt	25 kDa	28.0 ± 10.6	30.0 ± 9.9	29.7 ± 16.0
Aflatoxin B1 aldehyde reductase member 2	ARK72_RAT	Q8CG45	Akr7a2	41 kDa	35.3 ± 17.6	25.7 ± 5.0	23.3 ± 5.2
Phosphatidylethanolamine-binding protein 1	PEBP1_RAT	P31044	Pebp1	21 kDa	49.3 ± 35.5	10.7 ± 10.7	24.0 ± 9.0
UDP-glucose dehydrogenase, isoform CRA_a	G3V6C4_RAT	G3V6C4	Ugdh	55 kDa	21.7 ± 4.4	29.3 ± 4.2	31.7 ± 13.2
Elongation factor 2	EF2_RAT	P05197	Eef2	95 kDa	24.3 ± 7.5	38.3 ± 2.8	20.0 ± 9.2
Uncharacterized protein (Fragment)	F1LRJ9_RAT	F1LRJ9	Selenbp1	52 kDa	19.7 ± 7.7	28.0 ± 14.0	33.0 ± 8.0
V-type proton ATPase subunit B, brain isoform	VATB2_RAT	P62815	Atp6v1b2	57 kDa	27.7 ± 12.5	33.0 ± 5.7	18.0 ± 2.6
Uncharacterized protein	D3ZR01_RAT	D3ZR01	Gm2a	21 kDa	27.3 ± 5.0	28.0 ± 8.6	23.0 ± 8.1
Peroxisomal acyl-coenzyme A oxidase 1	ACOX1_RAT	P07872	Acox1	75 kDa	21.7 ± 0.9	30.7 ± 5.2	24.3 ± 4.9
Omega-amidase NIT2	NIT2_RAT	Q497B0	Nit2	31 kDa	40.0 ± 23.9	21.3 ± 11.1	9.0 ± 2.1
Serine hydroxymethyltransferase	Q6TXG7_RAT	Q6TXG7	Shmt1	75 kDa	25.0 ± 3.2	36.0 ± 14.7	8.3 ± 1.2
Malate dehydrogenase, mitochondrial	MDHM_RAT	P04636	Mdh2	36 kDa	16.0 ± 3.0	34.7 ± 6.1	18.0 ± 11.5
Peroxisomal multifunctional enzyme type 2	DHB4_RAT	P97852	Hsd17b4	79 kDa	22.0 ± 10.6	7.3 ± 0.3	38.0 ± 22.2

Protein Name	UniProt Entry Name	UniProt Accession	Gene Name	Molecular Weight	Mean Spectral Counts ± SEM		
					Control	1 Day	7 Day
Peroxiredoxin-1	PRDX1_RAT	Q63716	Prdx1	22 kDa	27.0 ± 1.0	21.3 ± 12.1	18.7 ± 2.0
Spectrin alpha chain, brain	SPTA2_RAT	P07632	Sptan1	285 kDa	22.0 ± 10.3	25.0 ± 10.2	19.7 ± 10.7
Fructose-bisphosphate aldolase A	ALDOA_RAT	P05065	Aldoa	39 kDa	17.3 ± 5.5	28.0 ± 7.9	21.3 ± 5.5
Profilin-1	PROF1_RAT	P62963	Pfn1	15 kDa	31.7 ± 13.5	16.0 ± 8.1	16.3 ± 4.8
Aldose 1-epimerase	GALM_RAT	Q66HG4	Galm	38 kDa	20.3 ± 10.6	21.7 ± 8.0	22.0 ± 10.0
Uncharacterized protein	G3V8Z2_RAT	G3V8Z2	Xpnpep1	75 kDa	18.3 ± 4.5	25.0 ± 6.4	14.3 ± 7.4
Carbonic anhydrase 2	CAH2_RAT	P27139	Ca2	29 kDa	24.0 ± 8.5	21.7 ± 8.1	10.0 ± 6.0
Spectrin beta 2, isoform CRA_a	G3V6S0_RAT	G3V6S0	Sptbn1	274 kDa	14.0 ± 9.5	17.0 ± 2.6	22.3 ± 12.0
RCG52629	D4A133_RAT	D4A133	Atp6v1a	68 kDa	17.7 ± 6.7	21.3 ± 1.3	12.7 ± 5.4
Rab GDP dissociation inhibitor alpha	GDIA_RAT	P50398	Gdi1	51 kDa	17.7 ± 9.1	18.7 ± 1.9	15.0 ± 7.2
Nicotinate phosphoribosyltransferase domain containing 1, isoform CRA_c	G3V709_RAT	G3V709	Naprt1	59 kDa	17.0 ± 7.8	26.3 ± 8.2	7.3 ± 4.3
Phenylalanine-4-hydroxylase	PH4H_RAT	P04176	Pah	52 kDa	22.0 ± 2.9	11.7 ± 3.0	15.7 ± 2.0
D-amino-acid oxidase	OXDA_RAT	O35078	Dao	39 kDa	21.3 ± 9.8	14.0 ± 8.1	12.0 ± 4.2
Delta-aminolevulinic acid dehydratase	HEM2_RAT	P06214	Alad	36 kDa	20.3 ± 13.4	20.3 ± 13.3	6.0 ± 3.2
Phosphoglycerate mutase 1	PGAM1_RAT	P25113	Pgam1	29 kDa	20.3 ± 9.8	16.0 ± 6.0	10.3 ± 1.3
40S ribosomal protein S24	D4A6H5_RAT	D4A6H5	Rps24	15 kDa	21.0 ± 8.7	8.0 ± 4.0	16.7 ± 8.4
Similar to RIKEN cDNA C630028N24 gene (Predicted), isoform CRA_b	D3ZUX1_RAT	D3ZUX1	Agphd1	42 kDa	12.3 ± 4.1	15.7 ± 0.9	17.0 ± 7.5
Similar to Glutathione S-transferase, theta 3 (Predicted)	D3Z8I7_RAT	D3Z8I7	Gstt1	23 kDa	10.0 ± 3.1	14.7 ± 0.7	20.3 ± 11.7
D-3-phosphoglycerate dehydrogenase	SERA_RAT	O08651	Phgdh	56 kDa	16.3 ± 7.3	19.3 ± 2.4	8.0 ± 2.3
Cytosolic 10-formyltetrahydrofolate dehydrogenase	AL1L1_RAT	P28037	Aldh1l1	99 kDa	11.0 ± 4.6	19.0 ± 6.1	12.7 ± 4.8
T-complex protein 1 subunit epsilon	TCPE_RAT	Q68FQ0	Cct5	60 kDa	14.3 ± 2.3	14.3 ± 5.7	14.0 ± 10.0
Cullin-associated NEDD8-dissociated protein 1	CAND1_RAT	P97536	Cand1	136 kDa	15.7 ± 5.9	12.3 ± 2.9	14.0 ± 6.7
Isocitrate dehydrogenase [NADP], mitochondrial	IDHP_RAT	P56574	Idh2	51 kDa	8.0 ± 4.9	23.3 ± 7.4	10.7 ± 6.2
Acetyl-CoA acetyltransferase, mitochondrial	THIL_RAT	P17764	Acat1	45 kDa	13.3 ± 6.6	21.3 ± 8.2	5.7 ± 3.3
60S acidic ribosomal protein P0	RLA0_RAT	P19945	Rplp0	34 kDa	17.3 ± 2.3	7.0 ± 2.1	15.7 ± 8.8
Uncharacterized protein (Fragment)	F1LW12_RAT	F1LW12	Mthfd1	100 kDa	17.3 ± 1.5	6.3 ± 4.4	16.3 ± 4.1
14-3-3 protein zeta/delta	1433Z_RAT	P63102	Ywhaz	28 kDa	14.3 ± 6.7	16.3 ± 10.3	9.0 ± 8.0

Protein Name	UniProt Entry Name	UniProt Accession	Gene Name	Molecular Weight	Mean Spectral Counts ± SEM		
					Control	1 Day	7 Day
Dihydropteridine reductase	DHPR_RAT	P11348	Qdpr	26 kDa	15.0 ± 2.5	13.0 ± 4.4	10.7 ± 4.6
Isoform 2 of Cytosol aminopeptidase	AMPL_RAT	Q68FS4	Lap3	53 kDa	12.3 ± 6.7	20.3 ± 6.9	6.0 ± 2.9
Uncharacterized protein	F1LML2_RAT	F1LML2	Ubc	91 kDa	14.7 ± 7.8	16.0 ± 2.1	7.7 ± 0.7
Thiomorpholine-carboxylate dehydrogenase	CRYM_RAT	Q9QYU4	Crym	34 kDa	16.7 ± 15.7	10.3 ± 9.4	11.3 ± 5.5
RCG25819, isoform CRA_a	G3V9B9_RAT	G3V9B9	Acaa1a	45 kDa	13.7 ± 6.2	14.7 ± 5.9	9.7 ± 3.5
Guanine nucleotide-binding protein subunit beta-2-like 1	GBLP_RAT	P63245	Gnb2l1	35 kDa	9.7 ± 2.2	13.0 ± 6.8	15.3 ± 5.9
2-amino-3-carboxymuconate-6-semialdehyde decarboxylase	ACMSD_RAT	Q8R5M5	Acmsd	38 kDa	21.0 ± 11.2	12.0 ± 7.2	5.0 ± 2.5
Argininosuccinate lyase	ARLY_RAT	P20673	Asl	52 kDa	18.0 ± 7.6	9.7 ± 1.9	10.0 ± 1.7
Ester hydrolase C11orf54 homolog	CK054_RAT	Q5U2Q3	N/A	35 kDa	18.3 ± 11.7	8.7 ± 7.2	10.3 ± 1.9
Uncharacterized protein	F1LNM3_RAT	F1LNM3	Ank3	246 kDa	6.0 ± 3.8	15.3 ± 2.2	15.3 ± 6.2
Aldo-keto reductase family 1, member C1 (Dihydrodiol dehydrogenase 1; 20-alpha (3-alpha)-hydroxysteroid dehydrogenase)	Q3MHS3_RAT	Q3MHS3	Akr1c1	37 kDa	6.7 ± 1.3	19.7 ± 7.3	10.0 ± 3.1
Phosphotriesterase-related protein	PTER_RAT	Q63530	Pter	39 kDa	17.3 ± 12.9	8.3 ± 6.8	10.0 ± 4.7
Glutathione S-transferase alpha-4	GSTA4_RAT	P14942	Gsta4	26 kDa	6.0 ± 3.1	15.3 ± 3.4	13.3 ± 4.4
Glutathione peroxidase 1	GPX1_RAT	P04041	Gpx1	22 kDa	8.7 ± 4.6	17.7 ± 2.4	6.7 ± 1.5
Plasma glutamate carboxypeptidase	PGCP_RAT	P25113	Pgcp	52 kDa	6.7 ± 3.5	15.0 ± 5.3	11.3 ± 0.7
Chloride intracellular channel protein 1	CLIC1_RAT	Q6MG61	Clic1	27 kDa	8.7 ± 3.0	7.7 ± 4.7	16.3 ± 3.3
Uncharacterized protein (Fragment)	F1M668_RAT	F1M668	Grhpr	36 kDa	14.7 ± 7.5	9.3 ± 3.8	8.3 ± 6.4
Eukaryotic translation initiation factor 4A1	Q6P3V8_RAT	Q6P3V8	Eif4a1	46 kDa	6.0 ± 4.6	19.0 ± 4.4	7.3 ± 3.9
Isoform Cytoplasmic+peroxisomal of Peroxiredoxin-5, mitochondrial	PRDX5_RAT	Q9R063	Prdx5	17 kDa	13.3 ± 8.4	12.3 ± 6.4	6.3 ± 2.6
RCG52860, isoform CRA_b	G3V6C2_RAT	G3V6C2	Hgd	50 kDa	6.3 ± 1.7	17.3 ± 7.0	8.0 ± 1.0
Calbindin	CALB1_RAT	P07171	Calb1	30 kDa	24.7 ± 16.3	3.7 ± 2.3	2.7 ± 1.5
Uncharacterized protein	D3ZE63_RAT	D3ZE63	LOC686548	13 kDa	12.3 ± 7.5	14.0 ± 5.1	4.7 ± 3.7
Acyl-coenzyme A thioesterase 1	ACOT1_RAT	O88267	Acot1	46 kDa	15.3 ± 4.2	9.7 ± 3.7	6.0 ± 1.2
Ketohexokinase	KHK_RAT	Q02974	Khk	33 kDa	13.0 ± 5.1	8.3 ± 2.9	9.7 ± 3.5
Uncharacterized protein	D4A2P3_RAT	D4A2P3	Ptgr2	35 kDa	10.7 ± 5.7	14.0 ± 0.6	6.3 ± 1.9
Glyceraldehyde-3-phosphate dehydrogenase (Fragment)	F1M5I8_RAT	F1M5I8	N/A	36 kDa	11.7 ± 6.4	12.0 ± 7.9	7.3 ± 3.8

Protein Name	UniProt Entry Name	UniProt Accession	Gene Name	Molecular Weight	Mean Spectral Counts ± SEM		
					Control	1 Day	7 Day
Uncharacterized protein (Fragment)	F1LP60_RAT	F1LP60	Msn	68 kDa	9.7 ± 4.8	7.3 ± 4.3	14.0 ± 7.8
ADP-ribosylation factor 1	ARF1_RAT	P84079	Arf1	21 kDa	11.7 ± 6.6	13.0 ± 6.4	6.0 ± 5.0
Isoform 2 of Adenylate kinase 2, mitochondrial	KAD2_RAT	P29410	Ak2	26 kDa	11.0 ± 3.2	12.0 ± 1.2	7.7 ± 1.3
6-phosphogluconate dehydrogenase, decarboxylating	6PGD_RAT	P85968	Pgd	53 kDa	10.0 ± 3.5	10.7 ± 1.3	9.3 ± 6.4
Aldehyde dehydrogenase, mitochondrial	ALDH2_RAT	P11884	Aldh2	56 kDa	11.0 ± 7.1	15.0 ± 7.2	3.7 ± 2.7
Uncharacterized protein	D3Z936_RAT	D3Z936	Psmd12	45 kDa	19.7 ± 12.9	3.7 ± 3.7	5.7 ± 2.8
60 kDa heat shock protein, mitochondrial	CH60_RAT	P63039	Hspd1	61 kDa	4.7 ± 1.9	19.3 ± 6.4	5.0 ± 1.5
Na(+)/H(+) exchange regulatory cofactor NHE-RF1	NHRF1_RAT	Q9JJ19	Slc9a3r1	39 kDa	10.7 ± 5.2	9.3 ± 4.4	8.7 ± 0.9
Thioredoxin	THIO_RAT	P11232	Txn	12 kDa	14.0 ± 10.5	5.3 ± 2.0	9.0 ± 1.5
Glucosidase, beta, acid 3 (Cytosolic) (Predicted)	G3V8Y1_RAT	G3V8Y1	Gba3	33 kDa	14.3 ± 11.3	9.7 ± 3.8	4.3 ± 3.4
Uncharacterized protein (Fragment)	F1LQS6_RAT	F1LQS6	Xdh	135 kDa	4.7 ± 0.9	12.7 ± 4.1	10.7 ± 4.7
T-complex protein 1 subunit beta	TCPB_RAT	Q5XIM9	Cct2	57 kDa	17.3 ± 13.8	8.3 ± 2.2	2.3 ± 0.9
UMP-CMP kinase	KCY_RAT	Q4KM73	Cmpk1	22 kDa	8.7 ± 2.9	11.3 ± 2.8	7.7 ± 3.3
Phosphoserine aminotransferase	E9PSV5_RAT	E9PSV5	Psat1	41 kDa	12.0 ± 8.6	9.7 ± 2.4	5.7 ± 1.8
40S ribosomal protein S3a	RS3A_RAT	P49242	Rps3a	30 kDa	6.3 ± 3.2	10.3 ± 2.8	10.7 ± 4.3
Protein phosphatase 2 (Formerly 2A), regulatory subunit A (PR 65), alpha isoform, isoform CRA_a	Q5XI34_RAT	Q5XI34	Ppp2r1a	65 kDa	7.3 ± 2.3	9.7 ± 1.5	10.0 ± 2.6
60S ribosomal protein L6	F1LQS3_RAT	F1LQS3	Rpl6	34 kDa	11.3 ± 3.8	5.0 ± 2.1	10.3 ± 7.4
14-3-3 protein epsilon	1433E_RAT	P62260	Ywhae	29 kDa	11.0 ± 7.4	12.3 ± 10.3	3.3 ± 1.7
N(G),N(G)-dimethylarginine dimethylaminohydrolase 1	DDAH1_RAT	O08557	Ddah1	31 kDa	10.3 ± 5.9	8.7 ± 5.4	5.7 ± 2.9
Cysteine conjugate-beta lyase 1, isoform CRA_a	G3V827_RAT	G3V827	Ccbl1	52 kDa	9.7 ± 5.2	14.0 ± 5.0	1.0 ± 0.6
Dihydrofolate reductase	DYR_RAT	Q920D2	Dhfr	22 kDa	6.3 ± 3.5	14.0 ± 2.9	4.3 ± 2.2
Uncharacterized protein	F1M8E9_RAT	F1M8E9	Lyz2	17 kDa	8.3 ± 2.3	11.0 ± 6.7	5.0 ± 3.5
RCG20221, isoform CRA_b	G3V6T1_RAT	G3V6T1	Copa	138 kDa	9.0 ± 1.0	4.7 ± 1.7	10.0 ± 9.0
Retinol-binding protein 4	RET4_RAT	P04916	Rbp4	23 kDa	3.7 ± 2.7	7.3 ± 2.0	12.7 ± 2.3
Isoform 2 of Endoplasmin	ENPL_RAT	Q66HD0	Hsp90b1	74 kDa	8.3 ± 1.8	9.7 ± 2.2	5.7 ± 3.5

Protein Name	UniProt Entry Name	UniProt Accession	Gene Name	Molecular Weight	Mean Spectral Counts ± SEM		
					Control	1 Day	7 Day
Ubiquitin-like modifier-activating enzyme 1	UBA1_RAT	Q5U300	Uba1	118 kDa	11.0 ± 7.1	7.3 ± 4.5	5.3 ± 5.3
Liver carboxylesterase 4	EST4_RAT	Q64573	N/A	62 kDa	8.0 ± 4.9	10.3 ± 9.4	5.3 ± 3.2
Transgelin-2	TAGL2_RAT	Q5XFX0	Tagln2	22 kDa	10.3 ± 2.7	9.3 ± 0.7	3.7 ± 0.9
Uncharacterized protein	F1LMP7_RAT	F1LMP7	Grn	57 kDa	7.7 ± 5.0	7.3 ± 2.0	8.3 ± 3.5
Retinol-binding protein 1	RET1_RAT	P02696	Rbp1	16 kDa	11.0 ± 5.7	2.7 ± 1.8	8.7 ± 4.1
Acyl-CoA-binding protein	ACBP_RAT	P11030	Dbi	10 kDa	9.0 ± 6.0	8.3 ± 2.3	5.0 ± 1.0
Adenine phosphoribosyltransferase	APT_RAT	P36972	Aprt	20 kDa	9.0 ± 4.6	6.3 ± 2.6	6.7 ± 3.0
Uncharacterized protein	D3ZM33_RAT	D3ZM33	LOC100362298	18 kDa	6.0 ± 1.2	8.3 ± 2.2	7.7 ± 0.7
Uncharacterized protein	F2Z3T2_RAT	F2Z3T2	Tpm3	33 kDa	8.0 ± 1.0	11.0 ± 4.0	3.0 ± 1.7
Peroxisomal 2,4-dienoyl-CoA reductase	DECR2_RAT	Q9Z2M4	Decr2	31 kDa	5.0 ± 2.1	3.0 ± 3.0	13.7 ± 5.6
D-dopachrome decarboxylase	DOPD_RAT	P80254	Ddt	13 kDa	1.3 ± 1.3	2.7 ± 2.7	17.3 ± 8.4
Tissue-type transglutaminase	Q9WVJ6_RAT	Q9WVJ6	Tgm2	77 kDa	7.3 ± 1.9	11.7 ± 1.9	2.3 ± 1.9
Peroxiredoxin-6	PRDX6_RAT	O35244	Prdx6	25 kDa	12.0 ± 9.6	8.3 ± 5.3	0.3 ± 0.3
Glutathione S-transferase P	GSTP1_RAT	P04906	Gstp1	23 kDa	3.0 ± 0.6	6.7 ± 1.3	10.7 ± 3.4
40S ribosomal protein S4, X isoform	RS4X_RAT	P62703	Rps4x	30 kDa	9.0 ± 3.5	3.7 ± 0.3	7.7 ± 4.7
Biliverdin reductase A	BIEA_RAT	P46844	Blvra	34 kDa	2.3 ± 1.5	6.7 ± 1.2	11.3 ± 5.5
Ribosomal protein S5, isoform CRA_b	B0BN81_RAT	B0BN81	Rps5	23 kDa	8.3 ± 4.2	8.0 ± 4.4	4.0 ± 4.0
Low-density lipoprotein receptor-related protein 2	LRP2_RAT	P98158	Lrp2	519 kDa	12.3 ± 1.7	4.3 ± 2.4	3.3 ± 1.7
Uncharacterized protein (Fragment)	F1LM13_RAT	F1LM13	Ank3	195 kDa	6.0 ± 3.5	5.7 ± 5.7	7.7 ± 7.7
RCG29047, isoform CRA_b	G3V983_RAT	G3V983	Gstm1	26 kDa	3.0 ± 0.0	3.3 ± 3.3	13.0 ± 7.0
Napsin	Q9QX71_RAT	Q9QX71	Napsa	46 kDa	6.3 ± 2.3	7.7 ± 2.6	5.3 ± 2.7
Quinone oxidoreductase	QOR_RAT	Q6AYT0	Cryz	35 kDa	9.0 ± 4.5	5.3 ± 2.9	4.7 ± 0.9
Uncharacterized protein (Fragment)	F1LWF9_RAT	F1LWF9	Acaa2	42 kDa	6.3 ± 4.9	11.3 ± 7.0	1.0 ± 0.6
RCG34378, isoform CRA_h	G3V957_RAT	G3V957	LOC100359960	29 kDa	4.3 ± 0.9	6.0 ± 0.6	8.0 ± 1.7
Keratin, type II cytoskeletal 5	K2C5_RAT	Q6P6Q2	Krt5	62 kDa	15.0 ± 12.1	2.0 ± 2.0	1.3 ± 1.3
Aconitate hydratase, mitochondrial	ACON_RAT	Q9ER34	Aco2	85 kDa	4.7 ± 4.2	11.7 ± 6.2	1.7 ± 0.9
Pyruvate carboxylase, mitochondrial	PYC_RAT	P52873	Pc	130 kDa	5.3 ± 2.3	8.0 ± 4.0	4.7 ± 2.2
Alcohol dehydrogenase 1	ADH1_RAT	P06757	Adh1	40 kDa	5.7 ± 3.5	8.0 ± 2.0	4.3 ± 3.0
Cytoplasmic dynein 1 heavy chain 1	DYHC1_RAT	P38650	Dync1h1	532 kDa	5.3 ± 2.4	6.3 ± 2.9	6.3 ± 2.8
Transaldolase	TALDO_RAT	Q9EQS0	Taldo1	37 kDa	4.7 ± 2.9	11.0 ± 2.1	2.0 ± 0.6

Protein Name	UniProt Entry Name	UniProt Accession	Gene Name	Molecular Weight	Mean Spectral Counts ± SEM		
					Control	1 Day	7 Day
Uncharacterized protein	D3ZNT9_RAT	D3ZNT9	Picalm	72 kDa	5.7 ± 1.9	9.3 ± 2.3	2.7 ± 1.5
Dipeptidyl peptidase 2	DPP2_RAT	Q9EPB1	Dpp7	55 kDa	4.0 ± 2.3	8.7 ± 1.3	5.0 ± 1.2
Uncharacterized protein (Fragment)	F1M225_RAT	F1M225	Rab1	23 kDa	3.7 ± 2.7	7.7 ± 5.2	6.3 ± 3.8
Adaptor protein complex AP-1, beta 1 subunit, isoform CRA_a	G3V9N8_RAT	G3V9N8	Ap1b1	105 kDa	7.0 ± 3.5	6.3 ± 2.4	4.3 ± 3.0
Alpha-centractin	ACTZ_RAT	P85515	Actr1a	43 kDa	6.3 ± 4.9	6.3 ± 2.8	5.0 ± 4.0
Beta-galactosidase	D3ZUM4_RAT	D3ZUM4	Glb1	73 kDa	6.7 ± 2.4	7.0 ± 1.5	3.7 ± 1.8
Betaine--homocysteine S-methyltransferase 1	BHMT1_RAT	O09171	Bhmt	45 kDa	3.3 ± 1.3	9.0 ± 1.0	5.0 ± 1.7
40S ribosomal protein S3	RS3_RAT	P62909	Rps3	27 kDa	5.0 ± 2.1	8.0 ± 3.2	3.7 ± 1.9
Programmed cell death 6-interacting protein	PDC6I_RAT	Q9QZA2	Pdcd6ip	97 kDa	5.0 ± 2.1	8.0 ± 3.5	3.7 ± 1.9
Uncharacterized protein	F1M9V7_RAT	F1M9V7	Npepps	103 kDa	6.0 ± 1.5	6.0 ± 2.6	4.7 ± 0.9
Aromatic-L-amino-acid decarboxylase	DDC_RAT	P14173	Ddc	54 kDa	4.3 ± 0.9	8.0 ± 0.6	4.3 ± 3.0
60S acidic ribosomal protein P1	RLA1_RAT	P19944	Rplp1	11 kDa	7.7 ± 0.3	4.0 ± 1.5	4.7 ± 2.3
Annexin A4	ANXA4_RAT	P55260	Anxa4	36 kDa	9.7 ± 6.5	4.7 ± 1.7	1.7 ± 0.9
T-complex protein 1 subunit delta	TCPD_RAT	Q7TPB1	Cct4	58 kDa	9.7 ± 5.2	3.3 ± 1.9	3.0 ± 1.0
Alanine--glyoxylate aminotransferase 2, mitochondrial	AGT2_RAT	Q64565	Agxt2	57 kDa	5.0 ± 3.5	9.7 ± 5.4	1.3 ± 0.3
Heterogeneous nuclear ribonucleoprotein K	HNRPK_RAT	P61980	Hnrnpk	51 kDa	9.0 ± 4.6	3.3 ± 2.8	3.3 ± 1.8
5-oxoprolinase	OPLA_RAT	P97608	Oplah	138 kDa	7.3 ± 5.4	6.3 ± 2.8	2.0 ± 0.6
Sodium/potassium-transporting ATPase subunit alpha-1	AT1A1_RAT	P06685	Atp1a1	113 kDa	13.7 ± 2.3	0.7 ± 0.3	1.0 ± 0.6
3-mercaptopyruvate sulfurtransferase	THTM_RAT	P97532	Mpst	33 kDa	8.0 ± 4.9	6.0 ± 2.9	1.3 ± 1.3
Uncharacterized protein	D3ZPL5_RAT	D3ZPL5	RGD1562953	30 kDa	2.7 ± 1.8	4.0 ± 2.3	8.3 ± 1.8
40S ribosomal protein SA	RSSA_RAT	P38983	Rpsa	33 kDa	6.0 ± 3.2	3.7 ± 0.3	5.0 ± 1.5
WD repeat-containing protein 1	WDR1_RAT	Q5RKI0	Wdr1	66 kDa	2.0 ± 1.5	10.7 ± 1.2	2.0 ± 1.5
Peroxiredoxin-2	PRDX2_RAT	P35704	Prdx2	22 kDa	7.0 ± 2.1	3.3 ± 3.3	4.3 ± 0.9
Myosin, heavy polypeptide 9, non-muscle	G3V6P7_RAT	G3V6P7	Myh9	226 kDa	4.3 ± 2.8	5.0 ± 0.6	5.3 ± 0.3
Uncharacterized protein	D3ZD13_RAT	D3ZD13	Flnb	278 kDa	5.7 ± 4.2	5.0 ± 1.0	3.7 ± 0.7
3-hydroxybutyrate dehydrogenase type 2	BDH2_RAT	D4A1J4	Bdh2	27 kDa	7.3 ± 3.0	4.3 ± 1.9	2.7 ± 1.8
Aspartoacylase-2	ACY3_RAT	Q5M876	Acy3	35 kDa	3.7 ± 0.3	2.7 ± 1.3	7.7 ± 3.8

Protein Name	UniProt Entry Name	UniProt Accession	Gene Name	Molecular Weight	Mean Spectral Counts ± SEM		
					Control	1 Day	7 Day
Dipeptidyl peptidase 3	DPP3_RAT	O55096	Dpp3	83 kDa	3.0 ± 0.6	7.0 ± 2.6	4.0 ± 2.1
Elongation factor 1-gamma	EF1G_RAT	Q68FR6	Eef1g	50 kDa	8.3 ± 4.6	5.0 ± 3.5	0.7 ± 0.7
RCG46686, isoform CRA_a	Q6PDV6_RAT	Q6PDV6	Rps14	16 kDa	5.0 ± 3.1	4.0 ± 1.5	5.0 ± 2.0
6-phosphogluconolactonase	6PGL_RAT	P85971	Pgls	27 kDa	7.0 ± 0.6	1.7 ± 0.3	5.0 ± 1.7
Uncharacterized protein	F1LNY0_RAT	F1LNY0	Hprt1	25 kDa	6.0 ± 3.0	2.0 ± 2.0	5.7 ± 1.8
Similar to RIKEN cDNA 2810055F11 (Predicted)	D3ZV91_RAT	D3ZV91	RGD1305721	38 kDa	4.7 ± 2.0	5.7 ± 3.2	3.3 ± 1.5
General vesicular transport factor p115	USO1_RAT	P41542	Uso1	107 kDa	4.0 ± 2.1	6.7 ± 1.9	2.7 ± 2.2
Uap1l1 protein	B5DEH4_RAT	B5DEH4	Uap1l1	56 kDa	8.0 ± 3.8	3.3 ± 0.9	2.0 ± 1.2
Isoform Short of 14-3-3 protein beta/alpha	1433B_RAT	P35213	Ywhab	28 kDa	1.3 ± 1.3	11.3 ± 6.8	0.7 ± 0.7
Uncharacterized protein	D3ZUL6_RAT	D3ZUL6	Acss2	79 kDa	3.3 ± 1.2	3.7 ± 1.8	6.0 ± 3.6
Rho GDP-dissociation inhibitor 1	GDIR1_RAT	Q5XI73	Arhgdia	23 kDa	7.3 ± 3.7	3.0 ± 1.5	2.7 ± 2.2
Actin-related protein 3	ARP3_RAT	Q4V7C7	Actr3	47 kDa	6.0 ± 3.0	2.7 ± 1.7	4.0 ± 2.1
RCG55135, isoform CRA_b	G3V852_RAT	G3V852	Tln1	270 kDa	4.0 ± 3.5	3.7 ± 2.0	5.0 ± 2.6
Uncharacterized protein (Fragment)	F1LQY0_RAT	F1LQY0	Gsr	46 kDa	3.0 ± 1.7	7.7 ± 2.9	2.0 ± 1.2
Peroxisomal bifunctional enzyme	ECHP_RAT	P07896	Ehhadh	79 kDa	6.7 ± 4.2	3.0 ± 0.6	3.0 ± 1.5
Stress-induced-phosphoprotein 1	STIP1_RAT	O35814	Stip1	63 kDa	3.3 ± 2.4	7.0 ± 2.6	2.3 ± 0.3
Uncharacterized protein	D4A6G6_RAT	D4A6G6	LOC100362339	16 kDa	4.3 ± 1.5	6.3 ± 0.3	2.0 ± 1.5
Glutamate dehydrogenase 1, mitochondrial	DHE3_RAT	P10860	Glud1	61 kDa	1.7 ± 0.7	6.3 ± 1.2	4.3 ± 2.0
RCG32401, isoform CRA_a	D3ZPA9_RAT	D3ZPA9	Ctsa	56 kDa	1.0 ± 0.0	10.0 ± 3.8	1.3 ± 0.9
Acidic leucine-rich nuclear phosphoprotein 32 family member A	AN32A_RAT	P49911	Anp32a	29 kDa	2.0 ± 1.5	8.3 ± 4.1	2.0 ± 1.5
T-complex protein 1 subunit alpha	TCPA_RAT	P28480	Tcp1	60 kDa	5.7 ± 4.2	3.7 ± 1.3	2.7 ± 2.2
Uncharacterized protein	G3V8A5_RAT	G3V8A5	Vps35	92 kDa	5.3 ± 2.6	4.0 ± 1.5	2.7 ± 1.7
Proteasome subunit alpha type	Q6P9V6_RAT	Q6P9V6	Psma5	26 kDa	4.7 ± 2.9	3.0 ± 1.7	4.3 ± 1.5
Uncharacterized protein	F1LRV4_RAT	F1LRV4	Hspa4	94 kDa	2.7 ± 1.8	6.0 ± 2.1	3.0 ± 0.6
Proteasome subunit beta type-2	PSB2_RAT	P40307	Psmb2	23 kDa	5.7 ± 2.3	2.3 ± 1.5	3.7 ± 2.7
Uncharacterized protein	G3V7T5_RAT	G3V7T5	Xylb	60 kDa	3.3 ± 1.2	8.0 ± 3.1	0.3 ± 0.3
Uncharacterized protein	D3ZGK1_RAT	D3ZGK1	Ddx19b	54 kDa	3.3 ± 1.7	4.0 ± 0.6	4.3 ± 3.0
Cystathionine gamma-lyase	CGL_RAT	P18757	Cth	44 kDa	3.3 ± 1.7	2.0 ± 0.0	6.3 ± 2.4
Uncharacterized protein	D3ZNG1_RAT	D3ZNG1	Gk	58 kDa	1.7 ± 0.3	3.7 ± 3.7	6.0 ± 0.6
Adenosylhomocysteinase	SAHH_RAT	P10760	Ahcy	48 kDa	6.7 ± 4.4	3.0 ± 3.0	1.7 ± 0.9

Protein Name	UniProt Entry Name	UniProt Accession	Gene Name	Molecular Weight	Mean Spectral Counts ± SEM		
					Control	1 Day	7 Day
Uncharacterized protein (Fragment)	F1LY12_RAT	F1LY12	N/A	33 kDa	5.0 ± 2.5	2.0 ± 2.0	4.3 ± 0.9
S-formylglutathione hydrolase	ESTD_RAT	B0BNE5	Esd	31 kDa	4.3 ± 2.2	5.3 ± 2.3	1.7 ± 0.9
Uncharacterized protein (Fragment)	F1M818_RAT	F1M818	Lztfl1	33 kDa	3.7 ± 2.3	4.7 ± 0.9	2.7 ± 1.3
Phosphoserine phosphatase	SERB_RAT	Q5M819	Psph	25 kDa	9.0 ± 5.1	1.0 ± 0.6	1.0 ± 0.6
Fatty acid-binding protein, heart	FABPH_RAT	P07483	Fabp3	15 kDa	6.3 ± 4.1	1.0 ± 1.0	3.7 ± 1.5
40S ribosomal protein S8	RS8_RAT	P62243	Rps8	24 kDa	3.7 ± 1.9	1.7 ± 0.9	5.3 ± 3.0
Keratin, type II cytoskeletal 1	K2C1_RAT	Q6IMF3	Krt1	65 kDa	6.0 ± 3.5	3.0 ± 3.0	1.7 ± 0.3
RCG30479, isoform CRA_b	B0K031_RAT	B0K031	Rpl7	30 kDa	6.7 ± 2.7	3.3 ± 2.8	0.7 ± 0.7
Translationally-controlled tumor protein	TCTP_RAT	P63029	Tpt1	19 kDa	1.7 ± 1.2	8.0 ± 1.5	1.0 ± 1.0
Uncharacterized protein	D3ZS68_RAT	D3ZS68	Pcbp1	37 kDa	3.0 ± 0.6	4.7 ± 2.3	3.0 ± 1.2
Prostaglandin E synthase 3	TEBP_RAT	P83868	Ptges3	19 kDa	1.0 ± 1.0	8.3 ± 0.9	1.3 ± 0.3
Delta-1-pyrroline-5-carboxylate dehydrogenase, mitochondrial	AL4A1_RAT	P0C2X9	Aldh4a1	62 kDa	1.3 ± 1.3	9.3 ± 5.0	0.0 ± 0.0
Nucleolin	NUCL_RAT	P13383	Ncl	77 kDa	0.7 ± 0.7	3.0 ± 0.6	6.7 ± 4.1
Uncharacterized protein	F2Z3Q8_RAT	F2Z3Q8	Kpnb1	97 kDa	3.3 ± 1.3	4.7 ± 0.9	2.3 ± 0.3
Isoform L-type of Pyruvate kinase isozymes R/L	KPYR_RAT	P12928	Pklr	59 kDa	4.7 ± 1.2	2.7 ± 0.7	2.7 ± 1.8
Enoyl-CoA hydratase, mitochondrial	ECHM_RAT	P14604	Echs1	32 kDa	2.7 ± 1.8	6.7 ± 4.4	0.7 ± 0.7
Phenazine biosynthesis-like domain-containing protein	PBLD_RAT	Q68G31	Pbld	32 kDa	3.7 ± 2.2	1.3 ± 0.9	5.0 ± 2.0
Uncharacterized protein	F1LQ78_RAT	F1LQ78	Renbp	50 kDa	5.3 ± 2.0	4.3 ± 2.2	0.3 ± 0.3
Legumain	LGMN_RAT	Q9R0J8	Lgmn	49 kDa	4.3 ± 2.6	3.3 ± 3.3	2.3 ± 2.3
Thioredoxin reductase 1, isoform CRA_a	G3V9V0_RAT	G3V9V0	Txnrd1	67 kDa	4.0 ± 2.6	4.7 ± 4.2	1.0 ± 1.0
Poly A binding protein, cytoplasmic 2 (Predicted)	D4A233_RAT	D4A233	Pabpc2	69 kDa	3.0 ± 1.5	4.0 ± 0.6	2.7 ± 1.7
Sodium/potassium-transporting ATPase subunit beta-1	AT1B1_RAT	P07340	Atp1b1	35 kDa	8.0 ± 3.2	1.7 ± 1.7	0.0 ± 0.0
Uncharacterized protein	D4ADE8_RAT	D4ADE8	Ddx3x	73 kDa	3.0 ± 0.6	3.3 ± 0.3	3.3 ± 3.3
Uncharacterized protein	D3Z8P5_RAT	D3Z8P5	RGD1566085	35 kDa	2.0 ± 1.0	5.3 ± 1.8	2.3 ± 1.9
Inositol oxygenase	MIOX_RAT	Q9QXN4	Miox	33 kDa	4.7 ± 0.9	2.3 ± 1.9	2.3 ± 1.9
Uncharacterized protein	D4A774_RAT	D4A774	N/A	11 kDa	0.3 ± 0.3	0.7 ± 0.7	8.3 ± 8.3
Glutamine synthetase	GLNA_RAT	P09606	Glul	42 kDa	7.3 ± 5.0	1.3 ± 1.3	0.7 ± 0.3

Protein Name	UniProt Entry Name	UniProt Accession	Gene Name	Molecular Weight	Mean Spectral Counts ± SEM		
					Control	1 Day	7 Day
Uncharacterized protein	D3ZW96_RAT	D3ZW96	Atp6v1h	56 kDa	3.7 ± 0.3	3.7 ± 2.7	1.7 ± 0.9
ATPase, H+ transporting, V1 subunit E isoform 1, isoform CRA_a	G3V7L8_RAT	G3V7L8	Atp6v1e1	26 kDa	3.0 ± 1.2	5.7 ± 1.8	0.3 ± 0.3
Bifunctional purine biosynthesis protein PURH	PUR9_RAT	O35567	Atic	64 kDa	5.7 ± 4.7	2.0 ± 1.5	1.3 ± 0.9
Chaperonin subunit 8 (Theta) (Predicted), isoform CRA_a	D4ACB8_RAT	D4ACB8	Cct8	60 kDa	2.3 ± 0.9	2.0 ± 1.2	4.3 ± 3.3
Proline synthetase co-transcribed (Predicted)	D3ZCA0_RAT	D3ZCA0	Prosc	30 kDa	3.3 ± 3.3	3.3 ± 3.3	2.0 ± 1.5
SEC31-like 1 (S. cerevisiae), isoform CRA_b	D3Z905_RAT	D3Z905	Sec31a	133 kDa	4.0 ± 0.6	2.7 ± 1.2	1.7 ± 1.2
Actin related protein 2/3 complex, subunit 4 (Predicted), isoform CRA_a	B2RZ72_RAT	B2RZ72	Arpc4	20 kDa	1.0 ± 1.0	3.7 ± 2.0	3.7 ± 1.9
Uncharacterized protein (Fragment)	F8WG98_RAT	F8WG98	Ak4	38 kDa	2.7 ± 0.9	4.7 ± 3.3	1.0 ± 0.6
Adenylyl cyclase-associated protein 1	CAP1_RAT	Q08163	Cap1	52 kDa	4.0 ± 2.1	4.0 ± 1.0	0.3 ± 0.3
Abhydrolase domain-containing protein 14B	ABHEB_RAT	Q6DGG1	Abhd14b	23 kDa	1.7 ± 0.9	2.7 ± 0.9	3.7 ± 1.9
Uncharacterized protein	D3ZGX5_RAT	D3ZGX5	N/A	49 kDa	4.0 ± 1.5	1.7 ± 0.7	2.3 ± 1.2
Epoxide hydrolase 2	HYES_RAT	P80299	Ephx2	62 kDa	1.0 ± 0.6	6.0 ± 4.2	1.0 ± 1.0
Isoamyl acetate-hydrolyzing esterase 1 homolog	IAH1_RAT	Q711G3	Iah1	28 kDa	2.3 ± 1.5	3.0 ± 1.2	2.7 ± 0.7
Uncharacterized protein	F2Z3T7_RAT	F2Z3T7	Isoc1	32 kDa	3.3 ± 1.8	1.7 ± 1.7	3.0 ± 0.6
Uncharacterized protein (Fragment)	F1LR40_RAT	F1LR40	Pepd	55 kDa	3.3 ± 1.5	2.7 ± 1.3	2.0 ± 1.0
Uncharacterized protein	D3ZY72_RAT	D3ZY72	LOC100363073	30 kDa	2.0 ± 0.6	4.0 ± 4.0	2.0 ± 1.2
Uncharacterized protein	D3ZH86_RAT	D3ZH86	N/A	100 kDa	1.7 ± 1.2	3.0 ± 1.0	3.3 ± 2.4
Beta-hexosaminidase subunit alpha	HEXA_RAT	Q641X3	Hexa	61 kDa	3.3 ± 2.0	1.7 ± 0.9	3.0 ± 1.5
Eukaryotic translation initiation factor 5A-1	IF5A1_RAT	Q3T1J1	Eif5a	17 kDa	1.3 ± 0.3	4.3 ± 0.9	2.3 ± 1.3
Uncharacterized protein	D3ZJM9_RAT	D3ZJM9	Gsto1	28 kDa	3.3 ± 1.3	1.7 ± 1.2	2.7 ± 0.9
Exportin-1	XPO1_RAT	Q80U96	Xpo1	123 kDa	3.0 ± 0.6	3.0 ± 1.7	1.7 ± 1.7
Uncharacterized protein	D3Z9J5_RAT	D3Z9J5	Vps26a	42 kDa	2.7 ± 0.9	3.3 ± 0.3	1.7 ± 1.2
Uncharacterized protein	D4A5F2_RAT	D4A5F2	Cep290	290 kDa	2.0 ± 0.6	2.3 ± 1.5	3.3 ± 1.8
26S proteasome non-ATPase regulatory subunit 2	PSMD2_RAT	Q4FZT9	Psmd2	100 kDa	3.3 ± 1.8	3.3 ± 1.5	1.0 ± 0.6

Protein Name	UniProt Entry Name	UniProt Accession	Gene Name	Molecular Weight	Mean Spectral Counts ± SEM		
					Control	1 Day	7 Day
Isoform III of Cystathionine beta-synthase	CBS_RAT	P32232	Cbs	60 kDa	4.0 ± 1.0	1.3 ± 0.7	2.3 ± 1.5
Cell division control protein 42 homolog	CDC42_RAT	Q8CFN2	Cdc42	21 kDa	5.0 ± 2.5	0.3 ± 0.3	2.3 ± 1.9
Purine nucleoside phosphorylase	PNPH_RAT	P85973	Pnp	32 kDa	3.7 ± 1.5	3.7 ± 2.3	0.0 ± 0.0
Serine/threonine-protein phosphatase 2A catalytic subunit alpha isoform	PP2AA_RAT	P63331	Ppp2ca	36 kDa	2.7 ± 1.8	2.7 ± 1.8	2.0 ± 1.2
Aldo-keto reductase family 1, member C12-like 1	A2VD16_RAT	A2VD16	Akr1c12l1	37 kDa	1.7 ± 1.2	3.3 ± 0.3	2.3 ± 1.5
Uncharacterized protein	D4A1Y4_RAT	D4A1Y4	Tom1	57 kDa	2.7 ± 1.5	3.7 ± 2.7	0.7 ± 0.7
Uncharacterized protein	D3ZUM0_RAT	D3ZUM0	Gstt1	28 kDa	2.7 ± 1.7	3.3 ± 1.2	1.0 ± 0.0
Chloride intracellular channel 4, isoform CRA_b	G3V8C4_RAT	G3V8C4	Clic4	29 kDa	2.0 ± 1.0	4.0 ± 2.5	1.0 ± 0.6
Pyruvate kinase isozymes M1/M2	KPYM_RAT	P11980	Pkm2	58 kDa	5.0 ± 3.2	1.3 ± 1.3	0.7 ± 0.3
Uncharacterized protein	D3ZN03_RAT	D3ZN03	LOC100362751	12 kDa	2.3 ± 1.5	1.7 ± 0.9	3.0 ± 2.1
Electron transfer flavoprotein subunit alpha, mitochondrial	ETFA_RAT	P13803	Etfa	35 kDa	2.3 ± 1.2	3.3 ± 3.3	1.3 ± 1.3
T-complex protein 1 subunit gamma	TCPG_RAT	Q6P502	Cct3	61 kDa	2.7 ± 1.5	2.3 ± 1.9	1.7 ± 0.3
Medium-chain specific acyl-CoA dehydrogenase, mitochondrial	ACADM_RAT	P08503	Acadm	47 kDa	2.0 ± 1.5	4.7 ± 3.3	0.0 ± 0.0
Adenylate kinase isoenzyme 1	KAD1_RAT	P39069	Ak1	22 kDa	2.7 ± 2.2	2.7 ± 1.8	1.3 ± 0.9
Acyl-coenzyme A synthetase ACSM2, mitochondrial	ACSM2_RAT	O70490	Acsm2	64 kDa	2.0 ± 2.0	4.0 ± 2.1	0.7 ± 0.3
Thioredoxin domain containing 17	B0K010_RAT	B0K010	Txndc17	14 kDa	4.3 ± 4.3	2.3 ± 2.3	0.0 ± 0.0
Glutaredoxin-3	GLRX3_RAT	Q9JLZ1	Glrx3	38 kDa	3.3 ± 2.3	2.3 ± 1.5	1.0 ± 0.6
3-hydroxyisobutyrate dehydrogenase, mitochondrial	3HIDH_RAT	P29266	Hibadh	35 kDa	1.3 ± 1.3	5.0 ± 2.1	0.3 ± 0.3
14-3-3 protein theta	1433T_RAT	P68255	Ywhaq	28 kDa	1.3 ± 1.3	5.3 ± 5.3	0.0 ± 0.0
Annexin A5	ANXA5_RAT	P14668	Anxa5	36 kDa	2.7 ± 2.7	2.7 ± 2.7	1.0 ± 0.6
AP-2 complex subunit alpha-2	AP2A2_RAT	P18484	Ap2a2	104 kDa	0.7 ± 0.7	2.3 ± 1.5	3.3 ± 1.8
Uncharacterized protein	E9PTS0_RAT	E9PTS0	Hnrnpab	36 kDa	1.3 ± 0.9	2.7 ± 1.5	2.3 ± 0.3
Uncharacterized protein	F1MAA7_RAT	F1MAA7	Lamc1	177 kDa	1.7 ± 1.2	1.7 ± 0.9	2.7 ± 2.7
Coatomer subunit gamma	COPG_RAT	Q66H80	Copg	98 kDa	2.7 ± 1.8	0.3 ± 0.3	3.0 ± 3.0
Vinculin	VINC_RAT	P85972	Vcl	117 kDa	2.3 ± 2.3	2.7 ± 1.5	1.0 ± 1.0

Protein Name	UniProt Entry Name	UniProt Accession	Gene Name	Molecular Weight	Mean Spectral Counts ± SEM		
					Control	1 Day	7 Day
Ras-related protein Rab-7a	RAB7A_RAT	P09527	Rab7a	24 kDa	2.0 ± 1.5	1.3 ± 1.3	2.7 ± 2.7
60S ribosomal protein L13	D4A075_RAT	D4A075	LOC100361259	24 kDa	0.7 ± 0.7	3.0 ± 1.2	2.0 ± 1.2
Uncharacterized protein	D3ZLL8_RAT	D3ZLL8	LOC100361715	15 kDa	0.7 ± 0.7	2.7 ± 1.5	2.3 ± 0.9
Aspartoacylase	ACY2_RAT	Q9R1T5	Aspa	35 kDa	1.7 ± 1.7	2.0 ± 0.0	2.0 ± 1.2
Uncharacterized protein	F1LNF7_RAT	F1LNF7	Idh3a	40 kDa	1.0 ± 1.0	3.0 ± 2.5	1.7 ± 1.7
Myosin regulatory light chain 12B	ML12B_RAT	P18666	Myl12b	20 kDa	0.3 ± 0.3	3.3 ± 1.9	2.0 ± 1.5
Sorting nexin-5	SNX5_RAT	B1H267	Snx5	47 kDa	2.0 ± 1.0	1.7 ± 0.9	1.7 ± 0.3
Phosphoglucomutase-1	PGM1_RAT	P38652	Pgm1	61 kDa	1.7 ± 1.2	3.7 ± 2.7	0.0 ± 0.0
ADP-ribosylation factor 4	ARF4_RAT	P61751	Arf4	20 kDa	2.7 ± 0.3	2.3 ± 1.2	0.3 ± 0.3
Arginyl-tRNA synthetase, cytoplasmic	SYRC_RAT	P40329	Rars	76 kDa	1.3 ± 1.3	2.7 ± 1.8	1.3 ± 0.7
Uncharacterized protein	F1LQI1_RAT	F1LQI1	Hagh	29 kDa	0.7 ± 0.3	2.3 ± 0.3	2.3 ± 0.9
Coatomer subunit delta	COPD_RAT	Q66H80	Arcn1	57 kDa	1.3 ± 0.9	2.3 ± 1.3	1.7 ± 1.2
Ubiquitin-conjugating enzyme E2M (UBC12 homolog, yeast) (Predicted), isoform CRA_a	D3ZNQ6_RAT	D3ZNQ6	Ube2m	21 kDa	0.7 ± 0.7	3.7 ± 0.3	0.7 ± 0.7
40S ribosomal protein S9	RS9_RAT	P29314	Rps9	23 kDa	1.7 ± 0.3	0.0 ± 0.0	3.3 ± 2.4
Uncharacterized protein	D4ABS2_RAT	D4ABS2	Dnm1l	81 kDa	2.0 ± 1.5	0.7 ± 0.7	2.3 ± 1.9
Uncharacterized protein	F1LNN9_RAT	F1LNN9	Basp1	22 kDa	2.0 ± 0.6	1.3 ± 1.3	1.7 ± 0.3
Glycine N-methyltransferase	GNMT_RAT	P13255	Gnmt	33 kDa	1.7 ± 1.2	2.0 ± 1.0	1.3 ± 1.3
Uncharacterized protein	D3ZZ99_RAT	D3ZZ99	Add1	73 kDa	1.3 ± 0.7	2.3 ± 0.9	1.3 ± 1.3
Uncharacterized protein	F1LPS8_RAT	F1LPS8	Pura	35 kDa	1.3 ± 0.9	2.7 ± 1.2	0.7 ± 0.7
Uncharacterized protein	F1LMJ9_RAT	F1LMJ9	Eprs	170 kDa	1.7 ± 1.2	1.0 ± 0.6	2.0 ± 2.0
Uncharacterized protein	D3ZF94_RAT	D3ZF94	Psmc3	50 kDa	1.7 ± 0.9	2.7 ± 1.8	0.3 ± 0.3
Hsc70-interacting protein	F10A1_RAT	P50503	St13	41 kDa	1.3 ± 1.3	2.7 ± 2.7	0.7 ± 0.3
Hsp90 co-chaperone Cdc37	CDC37_RAT	Q63692	Cdc37	45 kDa	1.3 ± 0.9	2.7 ± 1.8	0.7 ± 0.3
Glyoxalase domain-containing protein 4	GLOD4_RAT	Q5I0D1	Glod4	33 kDa	2.0 ± 1.5	2.7 ± 1.7	0.0 ± 0.0
Uncharacterized protein	D3ZZK1_RAT	D3ZZK1	LOC100359563	13 kDa	1.3 ± 0.7	2.3 ± 0.9	1.0 ± 0.0
RCG55994, isoform CRA_c	D4AC23_RAT	D4AC23	Cct7	60 kDa	2.0 ± 0.6	2.3 ± 1.5	0.3 ± 0.3
Isoform Non-brain of Clathrin light chain A	CLCA_RAT	P08081	Clta	24 kDa	2.3 ± 2.3	2.3 ± 2.3	0.0 ± 0.0
Uncharacterized protein	D3ZKG9_RAT	D3ZKG9	RGD1307222	151 kDa	1.0 ± 0.6	2.3 ± 1.2	1.3 ± 0.7

Protein Name	UniProt Entry Name	UniProt Accession	Gene Name	Molecular Weight	Mean Spectral Counts ± SEM		
					Control	1 Day	7 Day
Kynurenine/alpha-aminoadipate aminotransferase, mitochondrial	AADAT_RAT	Q64602	Aadat	48 kDa	1.0 ± 0.6	2.3 ± 0.9	1.3 ± 1.3
L-xylulose reductase	DCXR_RAT	Q920P0	Dcxr	26 kDa	1.3 ± 1.3	2.3 ± 2.3	1.0 ± 0.6
Annexin A11	Q5XI77_RAT	Q5XI77	Anxa11	54 kDa	2.3 ± 1.9	0.3 ± 0.3	2.0 ± 2.0
Uncharacterized protein	F1LPV0_RAT	F1LPV0	Nars	64 kDa	1.7 ± 0.9	2.0 ± 1.0	0.7 ± 0.7
Uncharacterized protein	D3ZWJ5_RAT	D3ZWJ5	LOC100359503	8 kDa	1.0 ± 1.0	2.7 ± 0.7	0.7 ± 0.7
Aspartate aminotransferase, cytoplasmic	AATC_RAT	P13221	Got1	46 kDa	1.0 ± 0.6	1.7 ± 1.7	1.7 ± 1.7
Carboxymethylenebutenolidase homolog	CMBL_RAT	Q7TP52	Cmbl	28 kDa	4.3 ± 2.6	0.0 ± 0.0	0.0 ± 0.0
Uncharacterized protein	D3Z8J0_RAT	D3Z8J0	RGD1564425	23 kDa	1.3 ± 0.7	2.0 ± 1.2	1.0 ± 1.0
Dynactin subunit 2	DCTN2_RAT	Q6AYH5	Dctn2	44 kDa	1.3 ± 1.3	2.0 ± 1.0	1.0 ± 1.0
Kinesin-1 heavy chain	KINH_RAT	Q2PQA9	Kif5b	110 kDa	0.7 ± 0.3	1.7 ± 1.2	1.7 ± 1.2
Uncharacterized protein	F1LP72_RAT	F1LP72	Eef1d	72 kDa	2.7 ± 1.5	1.0 ± 0.6	0.3 ± 0.3
Eukaryotic translation initiation factor 3 subunit A	EIF3A_RAT	Q1JU68	Eif3a	163 kDa	1.3 ± 0.9	0.7 ± 0.3	2.0 ± 2.0
High density lipoprotein binding protein	Q3KRF2_RAT	Q3KRF2	Hdlbp	142 kDa	0.0 ± 0.0	2.7 ± 2.2	1.3 ± 1.3
Uncharacterized protein	D3ZET5_RAT	D3ZET5	N/A	20 kDa	0.3 ± 0.3	0.0 ± 0.0	3.7 ± 2.7
Uncharacterized protein	D3ZE23_RAT	D3ZE23	Nap1l4	47 kDa	0.7 ± 0.7	2.0 ± 1.0	1.3 ± 1.3
AP-1 complex subunit mu-1	AP1M1_RAT	Q32Q06	Ap1m1	49 kDa	0.7 ± 0.7	1.0 ± 0.0	2.3 ± 0.9
Fumarate hydratase 1	Q5M964_RAT	Q5M964	Fh1	54 kDa	0.3 ± 0.3	3.0 ± 1.5	0.7 ± 0.7
Twinfilin-1	TWF1_RAT	Q5RJR2	Twf1	40 kDa	1.0 ± 0.6	2.3 ± 1.5	0.7 ± 0.7
Selenocysteine lyase	SCLY_RAT	Q68FT9	Scly	47 kDa	0.7 ± 0.7	1.0 ± 0.6	2.3 ± 1.5
Apoa1bp protein	B0BNM1_RAT	B0BN81	Apoa1bp	31 kDa	2.3 ± 0.9	1.7 ± 0.9	0.0 ± 0.0
Enolase (Fragment)	F1M9V3_RAT	F1M9V3	N/A	40 kDa	2.0 ± 2.0	1.0 ± 1.0	1.0 ± 1.0
3-hydroxyanthranilate 3,4-dioxygenase	3HAO_RAT	P46953	Haao	33 kDa	2.3 ± 1.2	1.3 ± 1.3	0.3 ± 0.3
Glutathione S-transferase theta-2	GSTT2_RAT	P30713	Gstt2	27 kDa	1.7 ± 0.9	1.0 ± 1.0	1.0 ± 0.6
Uncharacterized protein	D3Z982_RAT	D3Z982	N/A	29 kDa	1.3 ± 0.7	1.7 ± 1.7	0.7 ± 0.7
Dihydropyrimidinase	DPYS_RAT	Q63150	Dpys	57 kDa	0.7 ± 0.7	2.3 ± 0.3	0.7 ± 0.7
Acyl-coenzyme A thioesterase 8	ACOT8_RAT	Q8VHK0	Acot8	36 kDa	0.7 ± 0.7	1.0 ± 1.0	2.0 ± 1.5
Erythrocyte protein band 4.1-like 3	A3E0T0_RAT	A3E0T0	Epb4.1l3	97 kDa	1.0 ± 0.0	2.3 ± 0.3	0.3 ± 0.3
Ribosomal protein L15	D3ZU80_RAT	D3ZU80	RGD1560501	24 kDa	1.0 ± 0.6	0.3 ± 0.3	2.3 ± 1.5

Protein Name	UniProt Entry Name	UniProt Accession	Gene Name	Molecular Weight	Mean Spectral Counts ± SEM		
					Control	1 Day	7 Day
Lysyl-tRNA synthetase	D4ABR8_RAT	D4ABR8	Kars	68 kDa	1.0 ± 1.0	1.7 ± 1.7	0.7 ± 0.7
Similar to RIKEN cDNA 1810022C23	Q5M884_RAT	Q5M884	Eci3	34 kDa	2.0 ± 1.5	0.0 ± 0.0	1.3 ± 1.3
Uncharacterized protein	D4ACR0_RAT	D4ACR0	N/A	37 kDa	0.0 ± 0.0	0.0 ± 0.0	3.3 ± 1.8
Leukocyte elastase inhibitor A	ILEUA_RAT	Q4G075	Serpinb1a	43 kDa	1.0 ± 0.6	2.3 ± 1.5	0.0 ± 0.0
EH domain-containing protein 1	EHD1_RAT	Q641Z6	Ehd1	61 kDa	2.7 ± 2.2	0.3 ± 0.3	0.3 ± 0.3
Aspartyl aminopeptidase	Q4V8H5_RAT	Q4V8H5	Dnpep	53 kDa	0.3 ± 0.3	2.3 ± 2.3	0.7 ± 0.7
Uncharacterized protein	F8WG07_RAT	F8WG07	Calm1	21 kDa	0.7 ± 0.3	2.0 ± 1.2	0.3 ± 0.3
Aspartate aminotransferase, mitochondrial	AATM_RAT	P00507	Got2	47 kDa	1.0 ± 1.0	2.0 ± 0.6	0.0 ± 0.0
N-acetylgalactosamine kinase	GALK2_RAT	Q5XIG6	Galk2	50 kDa	0.0 ± 0.0	2.7 ± 1.5	0.3 ± 0.3
Proteasome (Prosome, macropain) 26S subunit, non-ATPase, 3	Q5U2S7_RAT	Q5U2S7	Psmd3	61 kDa	0.3 ± 0.3	1.7 ± 0.9	1.0 ± 0.6
Sorting nexin 2	B2RYP4_RAT	B2RYP4	Snx2	59 kDa	2.3 ± 1.5	0.7 ± 0.3	0.0 ± 0.0
Alanyl-tRNA synthetase, cytoplasmic	SYAC_RAT	P50475	Aars	107 kDa	2.0 ± 1.0	1.0 ± 1.0	0.0 ± 0.0
Uncharacterized protein	D4A6C5_RAT	D4A6C5	Arhgap1	51 kDa	0.7 ± 0.7	2.0 ± 2.0	0.3 ± 0.3
Uncharacterized protein	D3ZE37_RAT	D3ZE37	Rps11	19 kDa	1.7 ± 1.7	0.0 ± 0.0	1.3 ± 1.3
Uncharacterized protein	F1LP82_RAT	F1LP82	Rab2a	24 kDa	1.3 ± 0.9	0.3 ± 0.3	1.3 ± 1.3
Uncharacterized protein	D3ZEA8_RAT	D3ZEA8	N/A	920 kDa	0.3 ± 0.3	2.3 ± 2.3	0.3 ± 0.3
Uncharacterized protein (Fragment)	F1LRI5_RAT	F1LRI5	Gcn1l1	293 kDa	1.3 ± 0.9	0.7 ± 0.3	0.7 ± 0.3
Uncharacterized protein (Fragment)	F1M5X1_RAT	F1M5X1	Rrbp1	143 kDa	1.7 ± 1.7	1.0 ± 1.0	0.0 ± 0.0
Programmed cell death 6 (Predicted), isoform CRA_a	G3V7W1_RAT	G3V7W1	Pdcd6	22 kDa	1.7 ± 0.9	1.0 ± 0.6	0.0 ± 0.0
A-kinase anchor protein 2	AKAP2_RAT	Q5U301	Akap2	96 kDa	2.0 ± 1.5	0.7 ± 0.7	0.0 ± 0.0
ATP synthase subunit beta, mitochondrial	ATPB_RAT	P10719	Atp5b	56 kDa	1.3 ± 0.3	1.3 ± 0.9	0.0 ± 0.0
Uncharacterized protein	F1LQS4_RAT	F1LQS4	Acly	121 kDa	0.3 ± 0.3	1.0 ± 1.0	1.3 ± 1.3
26S protease regulatory subunit 4	PRS4_RAT	P62193	Psmc1	49 kDa	0.7 ± 0.7	0.7 ± 0.3	1.0 ± 1.0
Regucalcin	RGN_RAT	Q03336	Rgn	33 kDa	0.0 ± 0.0	0.7 ± 0.7	1.7 ± 1.7
Annexin A6	ANXA6_RAT	P48037	Anxa6	76 kDa	0.0 ± 0.0	1.3 ± 1.3	1.0 ± 1.0
Uncharacterized protein	D3ZF86_RAT	D3ZF86	RGD1309903	240 kDa	1.3 ± 1.3	0.3 ± 0.3	0.7 ± 0.7
Uncharacterized protein (Fragment)	F1M3T7_RAT	F1M3T7	Lrba	301 kDa	1.3 ± 1.3	0.3 ± 0.3	0.7 ± 0.7
Glutamate--cysteine ligase catalytic subunit	GSH1_RAT	P19468	Gclc	73 kDa	0.0 ± 0.0	2.0 ± 2.0	0.3 ± 0.3
Coatomer subunit beta	COPB_RAT	P23514	Copb1	107 kDa	1.3 ± 0.7	0.7 ± 0.7	0.3 ± 0.3
Uncharacterized protein (Fragment)	F1LMW6_RAT	F1LMW6	Psmd14	33 kDa	0.7 ± 0.7	1.3 ± 0.9	0.3 ± 0.3

Protein Name	UniProt Entry Name	UniProt Accession	Gene Name	Molecular Weight	Mean Spectral Counts ± SEM		
					Control	1 Day	7 Day
Uncharacterized protein (Fragment)	F8WFW6_RAT	F8WFW6	N/A	19 kDa	0.0 ± 0.0	1.0 ± 1.0	1.3 ± 1.3
Uncharacterized protein	F8WFK3_RAT	F8WFK3	Gsn	86 kDa	2.0 ± 1.2	0.0 ± 0.0	0.3 ± 0.3
Uncharacterized protein	D3ZBV7_RAT	D3ZBV7	Krt10	58 kDa	2.3 ± 2.3	0.0 ± 0.0	0.0 ± 0.0
Pyridoxine-5'-phosphate oxidase	PNPO_RAT	O88794	Pnpo	30 kDa	1.0 ± 1.0	1.0 ± 1.0	0.3 ± 0.3
Uncharacterized protein	D4AB03_RAT	D4AB03	Fam120a	122 kDa	2.0 ± 1.5	0.0 ± 0.0	0.3 ± 0.3
tRNA-splicing ligase RtcB homolog	RTCB_RAT	Q6AYT3	N/A	55 kDa	1.0 ± 1.0	0.0 ± 0.0	1.3 ± 0.9
Ubiquitin-conjugating enzyme E2 N	UBE2N_RAT	Q9EQX9	Ube2n	17 kDa	1.0 ± 1.0	1.3 ± 0.9	0.0 ± 0.0
Proteasome subunit alpha type-1	PSA1_RAT	P18420	Psma1	30 kDa	0.3 ± 0.3	1.3 ± 1.3	0.7 ± 0.7
Eukaryotic translation initiation factor 2 subunit 1	IF2A_RAT	P68101	Eif2s1	36 kDa	1.3 ± 1.3	0.7 ± 0.7	0.3 ± 0.3
Coatomer subunit beta'	COPB2_RAT	O35142	Copb2	103 kDa	0.7 ± 0.7	0.7 ± 0.7	0.7 ± 0.7
Coronin, actin-binding protein, 1B, isoform CRA_a	G3V940_RAT	G3V940	Coro1b	54 kDa	0.0 ± 0.0	1.7 ± 0.9	0.3 ± 0.3
Proteasome subunit alpha type-4	PSA4_RAT	P21670	Psma4	29 kDa	1.3 ± 1.3	0.0 ± 0.0	0.7 ± 0.3
Phospholipase A-2-activating protein	PLAP_RAT	P54319	Plaa	87 kDa	0.3 ± 0.3	0.7 ± 0.7	1.0 ± 1.0
Adenosylhomocysteinase	D3ZWL6_RAT	D3ZWL6	Ahcyl2	67 kDa	0.7 ± 0.3	1.0 ± 1.0	0.3 ± 0.3
Calpain-2 catalytic subunit	CAN2_RAT	Q07009	Capn2	80 kDa	0.7 ± 0.3	1.3 ± 1.3	0.0 ± 0.0
Protein disulfide-isomerase A3	PDIA3_RAT	P11598	Pdia3	57 kDa	1.3 ± 1.3	0.3 ± 0.3	0.3 ± 0.3
Uncharacterized protein	F1LQQ6_RAT	F1LQQ6	Pls1	70 kDa	1.3 ± 0.9	0.3 ± 0.3	0.3 ± 0.3
S-phase kinase-associated protein 1	SKP1_RAT	Q6PEC4	Skp1	19 kDa	1.3 ± 0.9	0.3 ± 0.3	0.3 ± 0.3
ATP-dependent RNA helicase DDX1	DDX1_RAT	Q641Y8	Ddx1	82 kDa	0.0 ± 0.0	1.0 ± 1.0	0.7 ± 0.3
Uncharacterized protein	D4ADG1_RAT	D4ADG1	N/A	309 kDa	0.0 ± 0.0	0.7 ± 0.3	1.0 ± 0.6
RNA-binding protein 47	RBM47_RAT	Q66H68	Rbm47	64 kDa	0.0 ± 0.0	1.0 ± 0.6	0.7 ± 0.3
Ornithine aminotransferase, mitochondrial	OAT_RAT	P04182	Oat	48 kDa	0.7 ± 0.7	1.0 ± 1.0	0.0 ± 0.0
Uncharacterized protein	D3Z976_RAT	D3Z976	N/A	99 kDa	0.7 ± 0.3	0.3 ± 0.3	0.7 ± 0.7
Myb-binding protein 1A	MBB1A_RAT	O35821	Mybbp1a	152 kDa	0.7 ± 0.7	0.7 ± 0.7	0.3 ± 0.3
Uncharacterized protein	D3ZRQ7_RAT	D3ZRQ7	N/A	136 kDa	0.7 ± 0.7	1.0 ± 1.0	0.0 ± 0.0
Dihydrolipoyllysine-residue acetyltransferase component of pyruvate dehydrogenase complex, mitochondrial	ODP2_RAT	P08461	Dlat	67 kDa	0.0 ± 0.0	0.7 ± 0.7	1.0 ± 1.0
Glycylpeptide N-tetradecanoyltransferase 1	NMT1_RAT	Q8K1Q0	Nmt1	57 kDa	0.0 ± 0.0	1.7 ± 0.3	0.0 ± 0.0
Eukaryotic translation initiation factor 3 subunit B	EIF3B_RAT	Q4G061	Eif3b	91 kDa	0.7 ± 0.7	1.0 ± 1.0	0.0 ± 0.0

Protein Name	UniProt Entry Name	UniProt Accession	Gene Name	Molecular Weight	Mean Spectral Counts ± SEM		
					Control	1 Day	7 Day
Uncharacterized protein (Fragment)	F1LM41_RAT	F1LM41	Mvp	97 kDa	1.3 ± 1.3	0.3 ± 0.3	0.0 ± 0.0
Annexin A1	ANXA1_RAT	P07150	Anxa1	39 kDa	0.0 ± 0.0	1.3 ± 1.3	0.3 ± 0.3
Uncharacterized protein	D4A5I9_RAT	D4A5I9	Myo6	146 kDa	0.3 ± 0.3	1.3 ± 0.9	0.0 ± 0.0
10 kDa heat shock protein, mitochondrial	CH10_RAT	P26772	Hspe1	11 kDa	0.3 ± 0.3	1.0 ± 1.0	0.3 ± 0.3
Heat shock protein 105 kDa	HS105_RAT	Q66HA8	Hsph1	96 kDa	0.3 ± 0.3	1.0 ± 0.6	0.3 ± 0.3
L-asparaginase	ASGL1_RAT	Q8VI04	Asrgl1	34 kDa	0.0 ± 0.0	0.3 ± 0.3	1.0 ± 1.0
Mitochondrial peptide methionine sulfoxide reductase	MSRA_RAT	Q923M1	Msra	26 kDa	1.0 ± 1.0	0.3 ± 0.3	0.0 ± 0.0
40S ribosomal protein S27-like	RS27L_RAT	P24051	Rps27l	9 kDa	1.3 ± 1.3	0.0 ± 0.0	0.0 ± 0.0
Uncharacterized protein	D4A0Y6_RAT	D4A0Y6	Mki67	348 kDa	0.3 ± 0.3	0.0 ± 0.0	1.0 ± 0.6
Alpha-soluble NSF attachment protein	SNAA_RAT	P54921	Napa	33 kDa	1.3 ± 1.3	0.0 ± 0.0	0.0 ± 0.0
Glutathione peroxidase	F1LPZ5_RAT	F1LPZ5	Gpx3	26 kDa	0.0 ± 0.0	1.3 ± 1.3	0.0 ± 0.0
Uncharacterized protein	F1LQS8_RAT	F1LQS8	Itpr1	313 kDa	0.3 ± 0.3	0.7 ± 0.7	0.0 ± 0.0
Uncharacterized protein	D3ZNH8_RAT	D3ZNH8	Pdcd11	208 kDa	0.7 ± 0.7	0.3 ± 0.3	0.0 ± 0.0
Uncharacterized protein (Fragment)	F1M6F4_RAT	F1M6F4	RGD1564597	14 kDa	0.3 ± 0.3	0.7 ± 0.7	0.0 ± 0.0
RCG21481, isoform CRA_b	D3ZLD5_RAT	D3ZLD5	Golga3	163 kDa	0.3 ± 0.3	0.7 ± 0.7	0.0 ± 0.0
Mitogen activated protein kinase kinase 7, isoform CRA_b	D3ZX58_RAT	D3ZX58	Map2k7	53 kDa	1.0 ± 1.0	0.0 ± 0.0	0.0 ± 0.0
Cubilin	CUBN_RAT	O70244	Cubn	399 kDa	0.3 ± 0.3	0.7 ± 0.7	0.0 ± 0.0
Ubiquitin carboxyl-terminal hydrolase	F1LM09_RAT	F1LM09	Usp7	128 kDa	0.3 ± 0.3	0.7 ± 0.7	0.0 ± 0.0
Srrm1 protein	B2RYB3_RAT	B2RYB3	Srrm1	102 kDa	0.0 ± 0.0	0.7 ± 0.7	0.0 ± 0.0
Sperm specific antigen 2 (Predicted)	D3ZLC3_RAT	D3ZLC3	Ssfa2	137 kDa	0.7 ± 0.7	0.0 ± 0.0	0.0 ± 0.0
Uncharacterized protein	D4A056_RAT	D4A056	N/A	7 kDa	0.0 ± 0.0	0.7 ± 0.7	0.0 ± 0.0
Keratin, type I cytoskeletal 17	K1C17_RAT	Q6IFU8	Krt17	48 kDa	0.7 ± 0.7	0.0 ± 0.0	0.0 ± 0.0
Uncharacterized protein	D3Z855_RAT	D3Z855	Tmem2	154 kDa	0.0 ± 0.0	0.0 ± 0.0	0.7 ± 0.7
Phenylalanyl-tRNA synthetase, beta subunit	Q68FT7_RAT	Q68FT7	Farsb	66 kDa	0.0 ± 0.0	0.0 ± 0.0	0.7 ± 0.7